Estimation of daily CO2 fluxes and of the components of the carbon budget for winter wheat by the assimilation of Sentinel 2-like remote sensing data into a crop model

Gaétan Pique, Rémy Fieuzal, Al Bitar Ahmad, Amanda Veloso, Tiphaine Tallec, Aurore Brut, Morgan Ferlicoq, Bartosz Zawilski, Jean-François Dejoux, Hervé Gibrin, et al.

Version of Record: https://www.sciencedirect.com/science/article/pii/S0016706119321998
Manuscript_d14652c728798515d4030e5a3f7fe5d9

Estimation of daily CO_2 fluxes and of the components of the carbon budget for winter wheat by the assimilation of Sentinel 2-like remote sensing data into a crop model

Pique Gaétan[(1,2)*], Fieuzal Rémy[(1)], Al Bitar Ahmad[(1)], Veloso Amanda[(1)], Tallec Tiphaine[(1)], Brut Aurore[(1)], Ferlicoq Morgan[(1)], Zawilski Bartosz[(1)], Dejoux Jean-François[(1)], Gibrin Hervé[(1)], Ceschia Eric[(3)]

[1]CESBIO, Université de Toulouse, CNES/CNRS/INRA/IRD/UPS, Toulouse, France
[2]Agence De l'Environnement et de Maîtrise de l'Energie (ADEME), Angers Cedex 1, France
[3]INRA, USC 1439 CESBIO, Toulouse, France

Keywords: crop modelling, carbon budget, remote sensing monitoring, winter wheat
* Corresponding author: E-mail address: piqueg@cesbio.cnes.fr

ABSTRACT

Croplands contribute to greenhouse gas emissions but also have the potential to mitigate climate change through soil carbon storage. However, there is a lack of tools based on objective observations for assessing cropland C budgets at the plot scale over large areas. Such tools would allow us to more precisely establish the contribution of an agricultural plot to net CO_2 emissions according to the plot management and identify levers for improving the C budget. In this study, we present a diagnostic regional modelling approach, called SAFY-CO_2, that assimilates high spatial and temporal resolution (HSTR) optical remote sensing data in a simple crop model and evaluate the performance of this approach in quantifying crop production and the main components of the annual carbon budget for winter wheat.

The SAFY-CO_2 model simulates daily crop development (biomass, partition to leaves, etc.), the components of net ecosystem CO_2 fluxes, and the annual yield and net ecosystem carbon budget (NECB).
Multi-temporal green area index (GAI) maps derived from HSTR data from the Formosat-2 and SPOT satellites were used to calibrate the light-use efficiency and phenological parameters of the model. Data from the literature were used to set a priori values for a set of model parameters, and a large dataset of in situ data was used for model validation. This dataset includes 8 years of eddy-covariance net CO_2 flux measurements and GAI, biomass and yield data acquired at 2 instrumented sites in southwest France. Biomass and yield data from 16 fields in the study area between 2005 and 2014 were also used for validation.
The SAFY-CO_2 model is able to reproduce both GAI dynamics (RRMSE=14%, R^2=0.97) and biomass production and yield (RRMSE of 27% and 21%, respectively) with high precisions under contrasting climatic, environmental and management conditions. Additionally, the net CO_2 flux components estimated by the model generally agreed well with in situ data and presented very good and significant correlations (RMSE of 1.74, 1.13 and 1.29 $gC.m^{-2}.d^{-1}$ for GPP, R_{eco} and NEE, respectively; R^2 of 0.90, 0.75 and 0.85 for GPP, R_{eco} and NEE, respectively) over the 8 studied years. This study also highlights the importance of accounting for post-harvest vegetative events (spontaneous re-growth, weed development and cover crops) for an accurate calculation of the annual net CO_2 flux. This approach requires a limited number of input parameters for estimating yield and net

CO_2 flux components, which is promising for regional/global-scale applications based on Sentinel 2-like data; however, the approach requires plot-scale data concerning organic amendments and straw management (exportation) in animal farming systems to calculate field C budgets.

1. INTRODUCTION

Agricultural lands occupy nearly 12% of Earth's terrestrial surface. They not only contribute to but also affect climate change because climatic conditions and water resources affect crop production (Smith et al., 2005). Additionally, the global food demand is increasing and may continue to increase for decades, driven by the increasing global population and per capita income that are anticipated through the middle of the next century (Tilman et al., 2011).

It is in this context that the '4 per mille Soils for Food Security and Climate' initiative was launched at COP21, with the aspiration to increase global soil organic matter stocks by 4 per 1000 (or 0.4%) per year as a compensation for part of the global emissions of greenhouse gases by anthropogenic sources and to increase food security (Chabbi et al., 2017; Minasny et al., 2017). Since then, this initiative has induced a wide debate in the scientific community concerning its feasibility (Baveye et al., 2018; Poulton et al., 2018), and it has been recognized that such an increase in soil organic carbon (SOC) is likely achievable in soils that are being actively managed for agriculture at a rate of increase that may not be achievable everywhere (Chabbi et al., 2017; Lal, 2016; Minasny et al., 2017; Pellerin et al., 2019). This debate illustrates the need for tools that can estimate changes in cropland SOC and identify potential levers to increase it. Currently, quantifying the net ecosystem carbon budgets (NECB) of croplands at regional or global scales remains difficult because of the heterogeneous character of agricultural landscapes, which have numerous plots with varied management practices and environmental conditions. This character results in uncertainties when assessing the impacts of specific management practices on the cropland NECB (Osborne et al., 2010) and when determining whether croplands are carbon sinks or sources (Ciais et al., 2010; West et al., 2010).

Indeed, the general biogeochemical models (such as SPA (Williams et al., 1996), Ecosys (Grant et al., 2007), Isba-Ags (Calvet et al., 1998), ORCHIDEE (Krinner et al., 2005), and ORCHIDEE-STICS (Gervois et al., 2008)) that are commonly used to simulate the carbon cycle in terrestrial ecosystems are not suited to account for the specificities and complexities of agro-ecosystems, particularly the effect of management practices. In contrast, the agronomic models or so-called crop models (*e.g.*, CERES (Gabrielle et al., 1998) or STICS (Brisson et al., 1998)) that account for management and pedoclimatic effects are primarily designed for simulating crop development and production (net primary production (NPP), yield) at the plot scale. However, unlike our approach, these models require information regarding management practices, which makes them less suitable for large spatial scale applications.

Several studies have demonstrated the benefit of assimilating remote sensing data into regional-scale crop models (Sus et al., 2013; Wu et al., 2012). In particular, the combination of high spatial and temporal resolution (HSTR) remote sensing data with crop models can provide, at the field scale over large areas, a timely and accurate picture of crop development (Claverie et al., 2012; Hadria et al., 2010), cropland photosynthesis (Wang et al., 2012; Wolanin et al., 2019) and net CO_2 fluxes (Revill et al., 2013; Sus et al., 2013). Among others, the SAFY (Duchemin et al., 2008; Claverie et al., 2012) and SAFY-WB (Battude et al., 2017; Duchemin et al., 2015) crop models constitute coherent frameworks for estimating biomass, yield production and water

requirements. These models describe the main biophysical processes underlying crop production by using climatic data and assimilate green area index (GAI) dynamic maps derived from remote sensing to avoid the need for management data, which makes them well suited for large-scale studies. In this work, we modified the SAFY model to simulate the components of the net ecosystem exchange (NEE) and to evaluate the potential of this approach for calculating cropland annual carbon budgets. The resulting model, called SAFY-CO_2, is described and evaluated against in situ data. The objectives of this study are as follows:

1- To assess the potential of an approach combining HSTR remote sensing data and a simple crop model to quantify the components of the NEE and of the annual NECB for winter wheat plots in contrasting climatic and management conditions.
2- To address the potentialities and limitations of such an approach in the perspective of future regional- or global-scale applications.

To fulfil our objectives, GAI maps derived from HSTR optical data (Formosat-2 and SPOT satellites) from 2006 to 2014 in southwestern France were used to constrain the photosynthetic light-use efficiency and phenological parameters of the model. Consequently, the simulated crop phenology agreed well with the satellite observations, which is essential for correctly estimating CO_2 fluxes and carbon budgets (Grant et al., 2007; Huang et al., 2009; Wattenbach et al., 2010).

A validation of the simulated CO_2 fluxes (photosynthesis, ecosystem respiration and NEE) was performed against eddy-covariance flux measurements that were carried out over two flux sites (Béziat, 2009) in the study area.

In the next section of the manuscript, the study area, experimental datasets and satellite database are presented. The following section describes the SAFY-CO_2 mathematical formulations, the parameterization and calibration procedure and the method for computing the annual NECB. The inputs required to run the model as well as the validation procedure are also detailed. Section 4 is dedicated to the results. The biomass and yield results are presented first, followed by the flux estimate results and finally the annual C budgets. Section five discusses the potentialities, the limitations and potential improvements of such an approach in the perspective of future regional- or global-scale applications. The paper ends with a conclusion concerning the main results, limitations and insights into future developments.

2. MATERIALS

2.1. Study area

The study area is part of the Regional Spatial Observatory [http://www.cesbio.ups-tlse.fr/fr/osr.html] located next to Toulouse in southwest France which includes 2 instrumented agricultural sites, Auradé (FR-Aur) and Lamasquère (FR-Lam) (Figure 1). Those two sites belong to the Integrated Carbon Observation System (ICOS) network [https://www.icos-ri.eu /] for observations of surface fluxes (CO_2, latent and sensible heat fluxes). The region has a temperate climate, with an annual mean precipitation of approximately 655 mm and an annual mean temperature of 12.9°C (measured by Meteo France at the Toulouse-Blagnac station between 1961 and 1990; see http://www.infoclimat.fr/climatologie/index.php). Agricultural activity occupies almost 90% of the landscape, and winter wheat is the main cultivated crop (covering approximately 20% of the total surface area). Sown from mid-October until the beginning of December, winter wheat is harvested from mid-June until the end of July, and straw is usually incorporated into the soil.

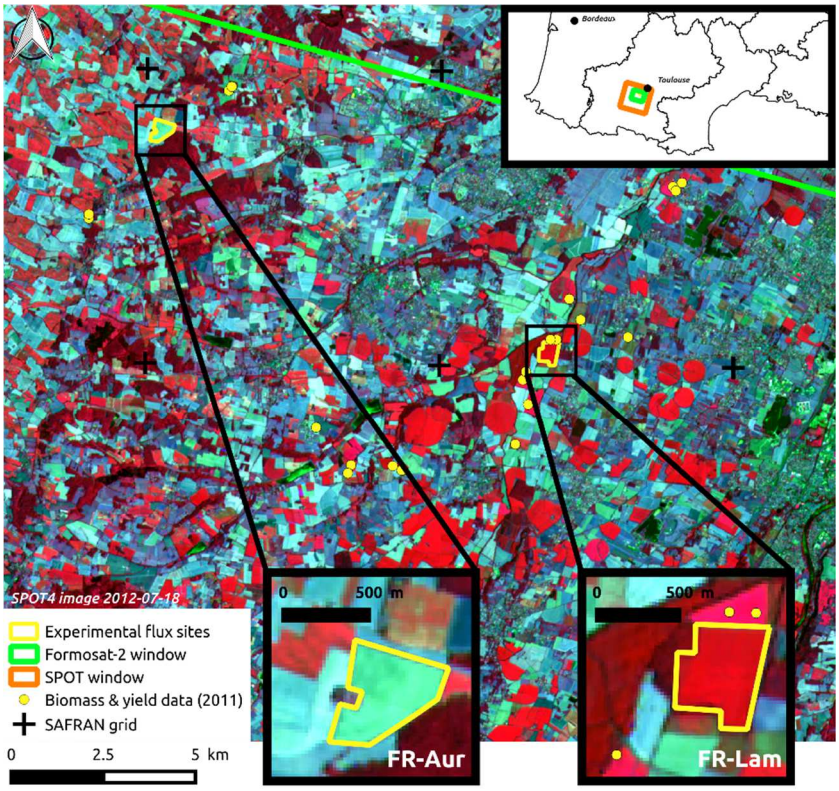

Figure 1: The upper right corner shows the location of the study site in southwestern France, as well as the footprint of Formosat-2 (green square) and Spot (orange square) images (in 2014 and 2012, respectively). The SPOT-4 false color image used as the background shows the flux sites of FR-Aur and FR-Lam (zoomed areas), the network of fields sampled for biomass and yield during the 2011 field campaign (yellow points), and the SAFRAN meteorological grid (black crosses).

2.1.1 Soil characteristics

The nature of the soils of the study area is shaped by the Garonne River. The Garonne River flows from the South to the North on the east side of the study area. It has spread sediments over a 15 km wide area along its western side resulting in vast terraces of heterogeneous soils called “boulbènes” and “terrefort” characterized by low-permeability and composed of a silt layer of variable thickness over stony clay soils. The geology is old quaternary and the main lithology is old alluviums. The area west of the terraces is characterized by a hilly landscape, consisting of hills and slopes resulting from the erosion of the oldest terraces. Further west the landscape is hilly over hundreds of kilometres and the soils become more calcareous with deposits formed of marl and clayey molasses with limestone.

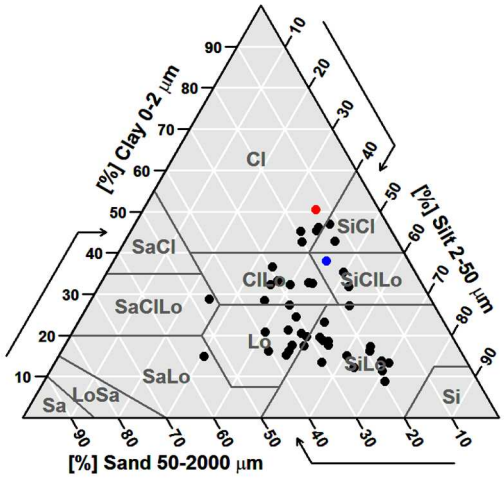

Figure 2: Surface texture measurements (FR-Lam in red, FR-Aur in blue and field campaign in black) displayed on USDA classification, with the following classes: clay (Cl), silty clay (SiCl), sandy clay (SaCl), clay loam (ClLo), silty clay loam (SiClLo), sandy clay loam (SaClLo), loam (Lo), silty loam (SiLo), sandy loam (SaLo), silt (Si), loamy sand (LoSa), sand (Sa).

The heterogeneous character of the soils of the study area is illustrated (Figure 2) by the texture measurements (fractions of clay, silt and sand) collected on the flux sites and on a network of fields within the footprint of the satellite images during the year 2018 (see also https://soilgrids.org/ for predicted soil classification of the study area). The texture

measurements are presented within the USDA triangle (United States Department of Agriculture, Figure 2). With fractions between 9 and 50% for the clay, between 25 and 72% for the silt and between 12 and 55% for the sand, the observed contents cover wide ranges of each component. On average, the texture is composed of 48% of silt and 26% of clay and sand, illustrating the dominance of silt fraction within the study area. FR-Lam soil is more clayey than the FR-Aur one and thus less permeable. As FR-Lam is located on the terraces near a river flood can occur after heavy rainfall. As the FR-Aur site is located on a hillside, its soil is heterogeneous and its depth vary from 1 to more than 2 m.

2.2. In situ data

The FR-Aur and FR-Lam sites have been intensively monitored since 2005. Micrometeorological, meteorological, soil and vegetation measurements are performed since then (see Béziat et al., 2009 for more details). Both sites have similar climatic conditions but different soil properties (see 2.1.1), topography and agricultural management practices. Winter wheat was cultivated throughout 8 cropping years, 2005-2006, 2009-2010, 2011-2012 and 2013-2014 at FR-Aur and 2006-2007, 2008-2009, 2010-2011 and 2012-2013 at FR-Lam. To facilitate the reading of this paper, we will identify each site-year by the three first letters of the site followed by the harvest year (*e.g.*, AUR2006 for the site-year 2005-2006 at Auradé).

The FR-Aur field (23.5 ha) is located on a hillside area near the Garonne River terraces and is characterized by a rapeseed/winter-wheat/sunflower/winter-wheat rainfed rotation that only receives mineral fertilizers. Only the grain is exported. The FR-Lam field (23.8 ha) is part of an experimental farm for milk and chicken production owned by the Purpan engineering school EIP (Ecole d'Ingénieurs de Purpan). It is characterized by a maize/winter-wheat rotation that is used to feed livestock and provide litter. Therefore, nearly all aboveground biomass is exported as grain and straw for winter wheat, and irrigated maize is harvested when it is still green for silage. Both organic and mineral fertilizers are applied.

A field campaign was conducted in June-July 2011 in 16 winter wheat fields to obtain spatially distributed in situ biomass and yield data (referred to as the '2011 field campaign'). The selection of fields was based on the analysis of the intra- and inter-field variability of the Normalized Difference Vegetation Index (NDVI derived from the Formosat-2 and SPOT optical images of April) to monitor a wide range of vegetation development. Crop biomass and yield measurements were performed just before the harvest.

2.2.1. GAI, biomass and yield data

Year	Site/ESU	Date of sowing	Date of harvest	Vegetation after harvest (nature)	GAI	Biomass	Grain yield	Flux and meteorological measurements
2006	AUR	27/10/2005	29/06/2006	Yes (weeds/re-growth)	9	9	F	Yes
2007	LAM	18/10/2006	15/07/2007	No	11	11	F	Yes
2009	LAM	19/11/2008	13/07/2009	Yes (weeds)	8	8	F	Yes
2010	AUR	19/11/2009	12/07/2010	No	5	5	F	Yes
2011	LAM	03/11/2010	02/07/2011	Yes (re-growth)	5	5	F	Yes
	Field Campaign	-	-	-	-	16	D	No
2012	AUR	21/10/2011	14/07/2012	No	5	5	F	Yes
2013	LAM	29/10/2012	22/07/2013	Yes (cover-crop)	5	5	F	Yes
2014	AUR	26/10/2013	10/07/2014	No	5	5	F	Yes

Table 1: Overview of the in situ data collected from 2005 until 2014, agricultural practices (dates of sowing harvest, etc.), and presence and type of vegetation during the fallow period. F: provided by farmer, D: destructive measurements.

During the vegetative cycle, the crop development at the experimental sites was regularly monitored using destructive measurements of GAI and dry aboveground mass (DAM) (see Béziat, 2009 for protocol), while yield data were provided by the farmers that cultivate the two flux sites. Farmer's data are often a mean of the yield at several fields surrounding the instrumented sites.

During the 2011 field campaign, biomass and yield data were collected from 16 fields according to the VALERI sampling protocol [http://w3.avignon.inra.fr/valeri/]. The samples were collected from five homogeneous square subplots inside the 16 Elementary Sampling Units (ESUs) of 20×20 m^2. The subplots sampled in each ESU were located in the ESU centre and corners. For each subplot, 4 rows with lengths of 50 cm and an inter-row distance of 13 cm were collected, which resulted in a sampling surface area of 0.25 m². The samples were dried and weighed, and the destructive grain yield was measured after threshing. The mean and associated standard deviations of the five subplots were calculated for each ESU.

Table 1 summarizes, for each year, the number and the kind of data that were acquired and it specifies if spontaneous regrowth, cover crop or weed development occurred or not after harvest for each year.

2.2.2. Flux and meteorological measurements

Turbulent fluxes of CO_2, water vapor (evapotranspiration and latent heat), sensible heat and momentum were measured continuously using the eddy-covariance (EC) method (Aubinet et al., 1999; Baldocchi, 2003; Moncrieff et al., 1997). The EdiRe software (Robert Clement, © 1999, University of Edinburgh, UK) was used to calculate the turbulent fluxes. The NEE was calculated as the sum of turbulent CO_2 fluxes and changes in CO_2 storage under the EC devices. Flux filtering, quality controls and gap filling were performed following the CarboEurope-IP recommendations ([www.carboeurope.org], see Béziat et al., (2009) for more details). The NEE was partitioned into gross primary production (GPP) and ecosystem respiration (R_{eco}) components according to the method proposed by Reichstein et al., (2005) and adapted by Béziat et al., (2009) for croplands (a process that could lead to over- or underestimations of the two components of the NEE). During the periods of bare soil, the GPP was set to 0, and the measured NEE fluxes only represented the R_{eco} component. Finally, the net ecosystem production (NEP) was derived from the annual integration of the NEE values. Synchronously, the standard meteorological variables were recorded at each experimental site and included different radiation components (*i.e.,* direct and diffuse components of incoming global radiation). After pre-processing, the semi-hourly fluxes and meteorological data were integrated or averaged at a daily time scale to be consistent with the model time step. Note that because of instrument failure, there was a 3-month gap in the flux measurements at the beginning of 2011 at FR-Lam.

For the '2011 field campaign' simulations, the SAFRAN meteorological data produced by Météo-France (Durand et al., 1993) are used. The SAFRAN data provide the air temperature, incoming global radiation, precipitation, and relative air humidity 2 m above the ground and the wind speed 10 m above the ground based on weather station measurements and modelling. The data are available every 6 h over an 8 km spatial resolution grid. The daily means of these climatic variables are calculated for each 2011 campaign field using bilinear interpolation. The other simulations are performed using the climatic data recorded at the instrumented sites.

During the studied years, the climatic conditions were very contrasted. The 2006-2007 cropping year was characterized by a mild winter resulting in strong vegetation developments while water stress occurred at the end of the 2005-2006 cropping season due to very low spring rainfall (86 mm at FR-Aur compared to 197 mm on

average over all studied years, see Béziat et al., 2009). The 2008-2009 autumn was characterized by heavy rainfall (cumulated precipitation of 192 mm during 2009 fall at FR-Lam compared to 154 mm in average between 2006 and 2014 at the same site) following the sowing, delaying crop emergence and resulting in very low biomass and yield production. The 2009-2010 cropping year was close to average in terms of precipitations and temperatures except during winter as temperatures were below the average (5.1°C at FR-Aur compared to 6.6°C on average) and were negative during several days resulting in two cumulated weeks delaying the crop development. In 2010-2011, the winter and spring were very dry (precipitation of 93 and 103 mm at FR-Lam in winter and spring respectively compared to 169 and 208 mm on average) delaying, crop development while hot temperatures in spring (average temperature of 16.5°C at FR-Lam during 2011 spring compared to 15.7°C on average during this period between 2006 and 2014) accelerated the development and the senescence. The cropping season 2011-2012 was characterized by a cold winter (mean temperature of 5.9°C at FR-Aur compared to an average of 6.6°C) during which low precipitations occurred (86 mm instead of 162 mm on average). In 2012-2013 heavy rainfall during winter and spring (323 and 296 mm at FR-Lam in winter and spring) coupled with hot temperatures in summer (21.1°C compared to a mean of 20.5°C) led to high biomass production. Finally, the cropping year 2013-2014 was characterized by its warm winter (8.1°C against 6.6°C on average) allowing the crop to start early in the season.

2.3. Satellite data and products

2.3.1. Multi-satellite optical images

This study uses an extensive dataset of HSTR from several satellites. Because of the spatial and temporal resolution of this dataset, and also as the bands necessary for this study are available from Sentinel-2 we consider that their combined used in this modelling exercise is representative of what could be achieved with Sentinel 2. Figure 3 presents a chronogram of the satellite images used in this study between 2006 and 2014. The images from those different satellites were combined to better monitor crop development and to reduce the gaps between successive observations. Nevertheless, the presence of clouds and/or shadows reduced the number of useful images. For instance, only one cloud-free SPOT image (April 26th) was available from mid-February until mid-June 2008; consequently, this site-year was not processed in the present study.

The high spatial resolution images provided by Formosat-2 (F2, 155 images) and Spot-2/4/5 (80 images) were in

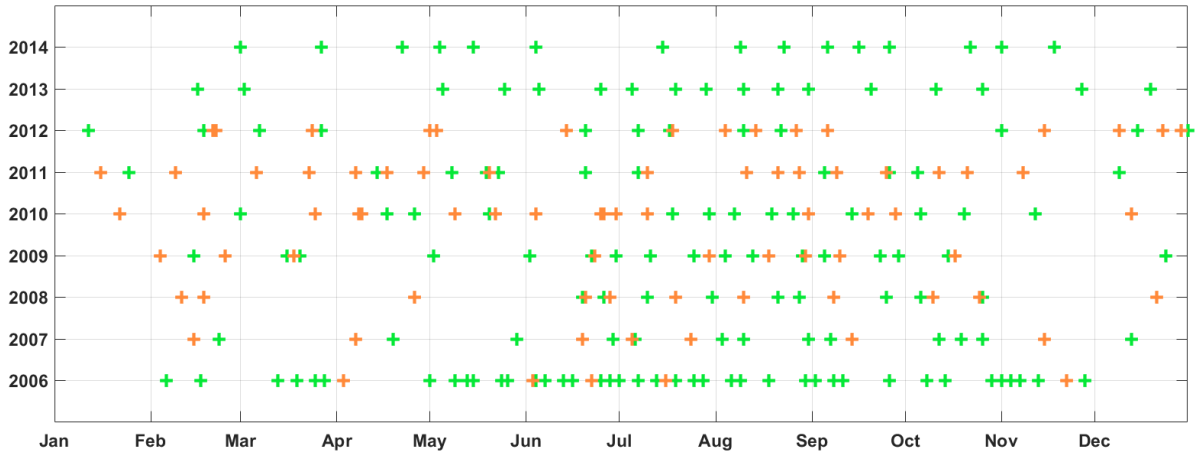

Figure 3: Timeline of the images acquired by Formosat-2 (green) and SPOT-2/4/5 (orange)

241 the optical domain (multispectral mode). The F2 images were characterized by a spatial resolution of 8 m
242 (footprint of 24×24 km^2) and were acquired at the same viewing angle (±45°) in four narrow wavelengths (blue,
243 green, red and near-infrared) (Chern et al., 2008). The SPOT images were characterized by spatial resolutions of
244 20 m (Spot-2/4) and 10 m (Spot-5) covering an area of 60 × 60 km^2. The images were acquired at two incidence
245 angles (75° and 102°) in at least three wavelengths (green, red, and near-infrared), with the medium-infrared
246 wavelength for SPOT-4/5 (Arnaud and Leroy, 1991).
247 Surface reflectances were derived from the satellite data using the KALIDEOS processing chain
248 [http://kalideos.cnes.fr] for atmospheric, radiometric and geometric corrections. The mean geometric correction
249 accuracy was close to 0.2 pixels (LaFrance, Lenot, Ruffel, Cao, & Rabaute, 2012), which is satisfactory for the
250 surface area of the studied fields.
251 The combined use of images acquired by different satellites was important to increase the number observations
252 per cropping year (see Figure 3). The comparison of the reflectances or of the NDVIs derived from different
253 sensors, including Formosat-2 and SPOT, acquired at close dates over various crops, had highlighted the good
254 performances of the processing chain and the limited effect of the sensor type (Battude et al., 2016; R. Fieuzal et
255 al., 2017).
256
257 *2.3.2. From image reflectance to GAI estimates*
258 The seasonal dynamic maps of GAI were derived from the surface reflectances using the BV-NNET tool
259 (Biophysical Variables Neural NETwork, Baret et al., (2007)), which consists of a trained artificial neural
260 network (ANN) using the outputs of a radiative transfer model (PROSAIL Jacquemoud et al., (2009)). ANNs
261 were first trained with the wide range of conditions estimated by the radiative transfer model. Then, the trained
262 network was used to predict the GAI from satellite reflectances. The GAI estimates derived from F2 and SPOT
263 reflectances were compared to non-destructive measurements based on digital hemispherical photographs
264 collected over a range of crops (Demarez et al., 2008) and showed a determination coefficient of $R^2 = 0.86$ and
265 an absolute root mean square error (RMSE) of approximately 0.5 $m^2.m^{-2}$ (Veloso, 2014). Battude et al., (2016)
266 also compared BV-NNET derived GAI from several satellites, including SPOT and Formosat-2. They showed
267 very good correlation (R=0.92 and RRMSE=23%) and performances that were similar to the ones found in the
268 literature (Berjón et al., 2013; Bsaibes et al., 2009; Duan et al., 2014). The BV-NNET procedure did not include
269 the aggregation of the leaves, which can lead to the underestimation of GAI during periods of strong vegetation
270 development (Claverie et al., 2012). GAI estimates were finally averaged considering all the pixels of the studied
271 plots after the application of an offset of 10 m to avoid edge effects and to consider only the GAI of the
272 considered crop.
273
274 **3. METHODOLOGY**
275 **3.1. The SAFY-CO_2 model**
276 The SAFY-CO_2 model (Figure 4) was adapted from the SAFY model (Simple Algorithm for Yield Estimates;
277 Duchemin et al., 2008) to simulate the components of the net CO_2 fluxes and the cropland annual carbon budget.
278 SAFY is a daily time step crop model that simulates the temporal evolution of GAI, DAM and final grain yield
279 (YLD) by considering two climatic input variables: incoming global radiation and mean temperature. This
280 approach is based on Monteith and Moss's (1977) light-use efficiency theory, which links the production of the

total DAM with the photosynthetically active portion of the solar radiation (PAR) absorbed by the plant. In SAFY, the ratio of photosynthesis to autotrophic respiration is assumed to be constant when estimating the DAM from the absorbed PAR (APAR). The SAFY model has been extensively used for the estimation of biomass and yield in contrasting climatic conditions and crop types (Battude et al., 2016; Claverie et al., 2012; Duchemin et al., 2015, 2008; Fieuzal et al., 2011).

Conversely, in SAFY-CO_2, the GPP is first estimated as a function of the APAR. Then, the components of the biomass (above and below ground) and the corresponding components of the net CO_2 fluxes and annual carbon budget are calculated. In this section, the main formalisms and equations of the model are presented and the parameters are detailed in the tables. Each table summarized the notations, the values or the ranges and the methods for estimating the parameters for the winter wheat crop and the post-harvest vegetative events.

First, the model computes photosynthesis (GPP) [eq.1] as a function of the incoming global radiation (R_g), the climatic efficiency (ε_c), the fraction of APAR by the plant (fAPAR) [eq.1.1], the temperature stress function (f_T) [eq.1.2], the effective efficiency of the conversion of absorbed radiation to fixed CO_2 through plant

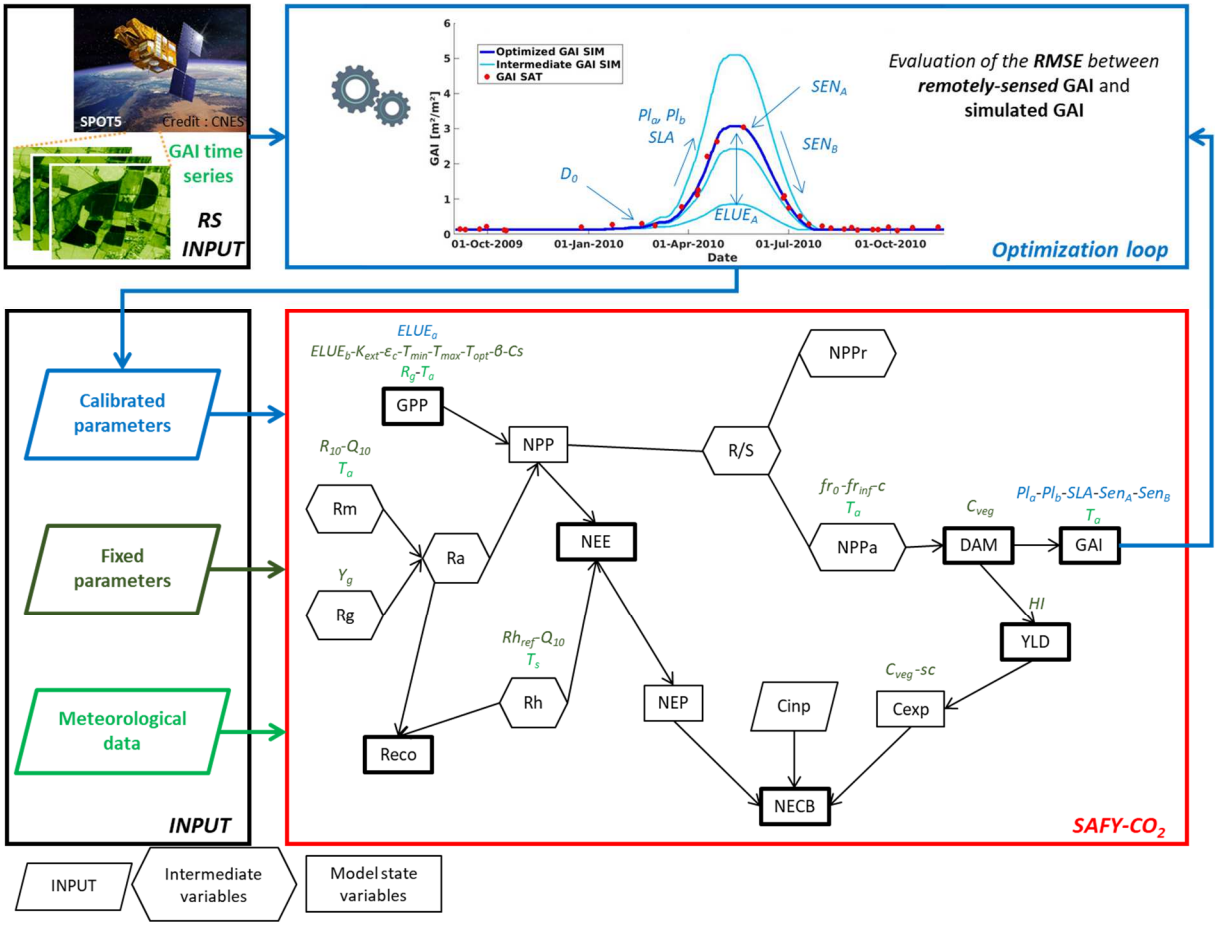

Figure 4: Schematic representation of the assimilation procedure of GAI derived from high resolution satellite optical images for the calibration of the agro-meteorological model SAFY-CO_2 by minimizing difference between satellite derived (SAT) and simulated (SIM) GAI. Also the figure shows the procedure for estimating the crop biomass, the components of the net CO_2 fluxes (GPP, R_{ECO}, NEE) and the annual carbon budgets (NECB) over a cropping season (see Tables 2 to 6 and equations 1 to 11.3.1 for more details concerning the processes simulated and the parameters).

294 photosynthesis (fELUE) [eq.1.3], and a multiplicative coefficient (sR10) [eq.1.4.1 and 1.4.2], which takes into
295 account the decline in canopy photosynthetic capacity during the senescence phase (see Béziat, 2009). sR10 is
296 set to 1 until senescence begins [eq.1.4.1] and then defined as the ratio between the GAI of the previous day and
297 the maximum seasonal GAI value multiplied by the corrective factor C_S. The senescence phase first acts on the
298 lower portion of the plant (closer to the soil) and then acts on the higher canopy elements. Thus, the actual
299 phenological senescence may be greater than the phenological senescence detected by satellite observations,
300 which thus requires a corrective factor. Therefore, the C_S coefficient is included in the computation of sR10 to
301 correct for the effects of senescence over simulated fluxes. The effects of diffuse global radiation over canopy
302 photosynthesis are not always considered in crop models when estimating crop productivity. However,
303 measurements, including the measurements at our flux sites, have indicated that the efficiency is very sensitive
304 to the diffuse components of incoming global radiation (Béziat, 2009; Hollinger et al., 1998; Roderick et al.,
305 2001). An effective light-use efficiency function is thus defined to account for the fraction of diffuse global
306 radiation (see 3.2). Because diffuse incoming radiation R_{df} is not often measured in the field, the De Jong (1980)
307 approach was used to estimate the R_{df}/R_g ratio over the study area from the top of the canopy and the top of the
308 atmosphere radiation data.

$$GPP = R_g * \varepsilon_c * fAPAR * f_T(T_a) * fELUE * sR10 \quad (1)$$

$$fAPAR = 1 - exp^{(-K_{ext}*GAI)} \quad (1.1)$$

$$f_T(T_a) = 1 - \left(\frac{T_{opt}-T_a}{T_{opt}-T_{min}}\right)^{\beta} \text{ for } T_{min} < T_a < T_{opt} \quad (1.2.1)$$

$$f_T(T_a) = 1 - \left(\frac{T_{opt}-T_a}{T_{opt}-T_{max}}\right)^{\beta} \text{ for } T_{opt} < T_a < T_{max} \quad (1.2.2)$$

$$f_T(T_a) = 0 \text{ for } T_a < T_{min} \text{ or } T_{max} < T_a \quad (1.2.3)$$

$$fELUE = ELUE_a * exp^{\left(ELUE_b * \frac{R_{df}}{R_g}\right)} \quad (1.3)$$

$$sR10 = 1 \text{ from sowing to senescence} \quad (1.4.1)$$

$$sR10 = \frac{GAI}{GAI_{max*Cs}} \text{ from senescence to harvest} \quad (1.4.2)$$

Description	Notation	Unit	Value/Range	Method	Source
Climatic efficiency	ε_c	-	0.48	Literature	Varlet-Grancher (1982)
Light-interception coefficient	K_{ext}	-	0.76	Literature	Veloso (2014)
Minimal temperature for growth	T_{min}	°C	0	Literature	(Porter and Gawith, 1999)
Maximal temperature for growth	T_{max}	°C	37	Literature	(Porter and Gawith, 1999)
Optimal temperature for growth	T_{opt}	°C	20	Literature	(Porter and Gawith, 1999)
Polynomial degree	β	-	2	Literature	Duchemin et al., 2008
Corrective factor over GPP during senescence	Cs	-	1.2	Flux data	-
Effective light-use efficiency parameter a	$ELUE_a$	gC.MJ^{-1}	[0.8-1.05] [0.5-0.8] (post-harvest vegetative events)	Calibration	-
Effective light-use efficiency parameter b	$ELUE_b$	-	1.34	Flux data	See supplementary material

Table 2. List of SAFY-CO_2 model parameters for calculating the GPP

The NPP is then derived from the difference between the GPP and the autotrophic respiration (R_a) [eq.2], which was separated into two components: maintenance respiration (R_m) and growth respiration (R_{gr}) (McCree, 1974) [eq.3]. R_m is calculated from the NPP of the previous day and a maintenance coefficient m_R [eq.3.1], which corresponds to the fraction of maintenance respiration per NPP unit. Because R_m responds strongly to the temperature (Amthor, 2000), it was estimated using a "Q_{10} type" equation (Van't Hoff, 1898) [eq.3.1.1]. In this equation, R_{10} is the reference respiration at 10°C. R_{gr} is calculated using the method described by Amthor (1989) and improved by Choudhury (2000), as shown in eq.3.2. The constant Y_g is the growth conversion efficiency.

$$NPP = GPP - R_a \quad (2)$$

$$R_a = R_m + R_{gr} \quad (3)$$

$$R_m = NPP * m_R * sR10 \quad (3.1)$$

$$m_R = R_{10} * Q_{10}^{\left(\frac{T_a - 10}{10}\right)} \quad (3.1.1)$$

$$R_{gr} = \left(1 - Y_g\right) * (GPP - R_m) \quad (3.2)$$

Description	Notation	Unit	Value/Range	Method	Source
Maintenance respiration parameter: Q_{10}	Q_{10}	-	2	Literature	Amthor 2000
Maintenance respiration parameter: R_{10}	R_{10}	g_C/g_{DM}	0.0025	literature	Béziat 2009
Growth respiration conversion efficiency parameter	Y_g	-	0.74	Literature	Amthor 1989

Table 3. List of SAFY-CO_2 model parameters for calculating autotrophic respiration

Finally, the total NPP is divided into root (NPP_r, [eq.4.1]) and aerial (NPP_a, [eq.4.2]) components, estimated by considering a root-to-shoot ratio (RtS) in accordance with the method proposed by Baret et al., (1992) [eq.5]. In this equation, SMT is the sum of temperature, D_0 is the emergence date and D_S is the first day of the spiking stage. fr_0 is the extrapolated value of the root fraction fr at emergence, fr_∞ is the asymptotic value of fr, and c is the relative rate of decrease. The DAM is estimated by dividing the NPP_a by the coefficient C_{veg}, which represents the plant carbon content [eq.6].

$$NPP_r = NPP * RtS \quad (4.1)$$

$$NPP_a = NPP * (1 - RtS) \quad (4.2)$$

$$RtS = fr = fr_\infty + (fr_0 - fr_\infty) * exp^{-c\left(\frac{SMT_{D_0}^{D_S} - SMT_{D_0}}{SMT_{D_S} - SMT_{D_0}}\right)} \quad (5)$$

$$DAM = \frac{NPP_a}{C_{veg}} \quad (6)$$

Description	Notation	Unit	Value/Range	Method	Source
Root fraction parameters	$f_0 - f_\infty - c$	-	0.63 / 0.11 / 1.48	Literature	Baret et al., 1992
Carbon content coefficient	C_{veg}	g_C/g_{veg}	0.46	Literature	Béziat 2009
Day of plant emergence	D_0	day	[20th Oct-15th Jan] [end of main crop-31th Dec] (post-harvest vegetative events)	Calibration	-

Table 4. List of SAFY-CO_2 model parameters for calculating the aboveground and the belowground mass

Once the biomass computed, the grain yield and GAI can be estimated, as in the SAFY version. The GAI is the sum of the GAI of the previous day and the positive and negative change in GAI of the current day [eq.7]. Leaf production and leaf senescence are controlled by a growing degree-day approach. The positive increment [eq.7.1] is the product of a function of leaf partitioning [eq.7.1.1], the specific leaf area parameter and the daily

DAM production. The negative increment, which is only evaluated from the beginning of senescence, depends on the two senescence parameters Sen_a and Sen_b [eq.7.2]. The grain yield estimation [eq.8] depends on the total biomass production at the end of the vegetative period (DAM_{max}) and a constant harvest index HI (see 3.2).

$$\Delta GAI = GAI + \Delta GAI^{+} - \Delta GAI^{-} \quad (7)$$

$$\Delta GAI^{+} = \Delta DAM * Pl * SLA \quad (7.1)$$

$$Pl = 1 - Pl_a * exp^{(Pl_b * SMT)} \quad (7.1.1)$$

$$\Delta GAI^{-} = GAI * \frac{SMT - Sen_a}{Sen_b} \quad (7.2)$$

$$Yield = DAM_{max} * HI \quad (8)$$

Description	Notation	Unit	Value/Range	Method	Source
Harvest index	HI	-	0.45	Literature	(Dai et al., 2016)
Specific leaf area	SLA	$m^2.g^{-1}$	[0.005 – 0.04]	Calibration	-
Partition-to-leaf function parameter a	Pl_a	-	[0.01-0.5]	Calibration	-
Partition-to-leaf function parameter b	Pl_b	-	[0.0001-0.02]	Calibration	-
Sum of temperature for senescence	Sen_a	°C	[1045-2000] [100-900] (post-harvest vegetative events)	Calibration	-
Rate of senescence	Sen_b	°C.day^{-1}	[10^3-2.10^4]	Calibration	-

Table 5. List of SAFY-CO_2 model parameters for calculating the leaf biomass production, the yield and the senescence

The NEE is calculated as the difference between the NPP and the carbon losses due to heterotrophic respiration (R_h) [eq.8]. R_h is calculated using a Q_{10} first-order exponential equation (Delogu, 2013). R_{href} is the reference respiration at 0°C, and exp^{b*10} is equal to Q_{10}.

The ecosystem respiration is defined as the sum of R_a and R_h [eq.10].

$$NEE = NPP - R_h \quad (8)$$

$$R_h = a * exp^{b*T_s} \quad (9)$$

$$a = R_{h_{ref}} \quad (9.1)$$

$$Q_{10} = \frac{Rh(T_s + 10)}{Rh(T_s)} = \frac{a * exp^{b*(T_s+10)}}{a * exp^{b*(T_s)}} = exp^{b*10} \quad (9.2)$$

$$R_{eco} = R_a + R_h \quad (10)$$

Description	Notation	Unit	Value/Range	Method	Source
Heterotrophic respiration parameter: Rhref	$R_{h_{ref}}$	gC.m^{-2}.d^{-1}	0.34	Literature	(Suleau et al., 2011)
Heterotrophic respiration parameter: Q_{10}	Q_{10}	-	2.3	Literature	(Suleau et al., 2011)
Conversion factor of Ta into Ts	t	-	1.07	ICOS sites data	-

Table 6. List of SAFY-CO_2 model parameters for calculating the heterotrophic respiration

3.2. Model parameterization and calibration

The parameters of the SAFY-CO_2 model are set using one of the following three options: i) literature sources, ii) multi-site in situ measurements and iii) optimization using the time series of satellite-derived GAI. The parameters in the first two categories are set as equal for all of the investigated fields and years of study (see equations 1 to 10 and Tables 2 to 6), while the parameter of the third category are optimized. Parameter b of the exponential function in the relationships between ELUE and R_{df}/R_g [eq.1.3] is fixed to 1.34 based on field data (*i.e.,* CO_2 fluxes and meteorological data) acquired over several years for contrasting climatic, soils, and management conditions at 5 European instrumented sites, including ours (Lonzee, BE; Auradé, FR; Grignon,

FR; Lamasquère, FR; Oensingen, CH; see Supplementary Material). This parameter is set to a generic value to facilitate the large-scale application of the approach.

The parameters in the third category are set using an iterative minimizing method with a RMSE objective function between satellite-based GAI and SAFY-CO_2 GAI estimates. This procedure aims at determining the values of parameter "a" of the fELUE function [eq.1.3] and 6 phenological parameters, *i.e.*, the day of plant emergence (D_0), the specific leaf area (SLA), the two parameters of the partition-to-leave function (Pl_a, Pl_b), the sum temperature for senescence (Sen_a) and the rate of senescence (Sen_b).

The minimization procedure, applied to each simulations (*i.e.* each cropping year and each field), is based on an adapted version of the Nelder-Mead simplex method (Lagarias et al., 1998), which considers a priori boundaries for each parameter to constrain the solutions within realistic parameter intervals. The minimization process runs the model, computes a cost function (in this case the RMSE derived from the comparison between the estimated and the remote sensed GAI) and iteratively updates the values of parameters to converge to the best parameter combination, coinciding with the lowest cost function value. To reduce the probability of local minima, a global approach is applied that runs the optimization process 30 times, with different *a priori* conditions for each parameter. A set of the parameters with the best solution is considered (*i.e.*, lower RMSE for the GAI estimates). The number of optimization runs is set to 30, based on a sensibility analysis, so that the best combination of parameters is always retrieved, while avoiding unnecessary runs.

The optimization process requires boundaries for the parameters to calibrate (Pl_a, Pl_b, Sen_a, Sen_b, SLA, $ELUE_a$, D_0). These boundaries are first estimated based on a literature review. Then, a sensitivity analysis of the model is conducted to adjust these boundaries using a grid search. The ranges of the parameters are discretized, and all possible combinations are simulated (more than 3 million simulations). Then, the outputs are compared to the outputs obtained by optimizations performed using the adapted simplex method described above and the same parameter boundaries. This comparison allows us to do the following.

1- Verify that the adjusted boundaries reproduce all plant development conditions, with the constraint of a limited dispersion in the outputs.

2- Validate the efficiency of the adapted version of the simplex in retrieving the best set of parameters.

Compared to SAFY, the SAFY-CO_2 version considers the biomass production of re-growth, weeds and cover crops (hereafter called post-harvest vegetative events) and their effect on the CO_2 fluxes and annual C budgets. Indeed, these post-harvest events can have an important impact on the NEE (Béziat et al., 2009; Ceschia et al., 2010; Poeplau and Don, 2015) and thus on the NECB. Therefore, the model is adapted to simulate these events without the distinction of their nature (*i.e.*, spontaneous re-growth, weeds or cover crop).

In a first attempt to estimate the effects of post-harvest vegetative events on the net CO_2 flux components and ultimately on the annual NECB, the same parameterization considered for winter wheat is also considered for all post-harvest vegetative events. For the studied years, when the satellite-derived GAI indicates the presence of vegetation on the field after harvest (*i.e.*, AUR2006, LAM2009, LAM2011, and LAM2013), the model is first run to simulate the main crop. Then, a second optimization is performed on the vegetation following the main crop, optimizing $ELUE_a$ and the 6 phenological parameters. The boundaries of parameters Sen_a, D_0 and $ELUE_a$ are changed compared to those fixed for winter wheat, while the ranges of the 4 other parameters remain the same.

3.3. From daily net ecosystem CO_2 fluxes, NEE to the annual net ecosystem carbon budget, NECB

To compute the annual NECB [eq.11], carbon input (C_{inp}) and export (C_{exp}) terms are added to the annual cumulated NEE (*i.e.,* the NEP) [eq.11.1]. The NEP is the carbon absorbed or released by the field (through photosynthesis and respiration processes) over a cultural year, a positive NEP indicates that cumulated soil and autotrophic respiration are higher than cumulated photosynthesis, meaning that the field loses carbon towards the atmosphere and vice versa. The value of NEP is computed from October 1st to September 30th because this period usually corresponds to the agricultural cropping year in Europe (Ceschia et al., 2010). The term C_{inp} represents the amount of C that is brought to the field as organic fertilizer (only at FR-Lam in this study) and as seeds. Since C_{inp} could not be simulated, the C_{inp} values provided by the farmer as well as analysis of the organic fertilizer C content (Béziat et al., 2009), were used to calculate the NECB at LAM.

C_{exp} generally corresponds to the yield [eq.11.2] in the study area, as typically, only grain is exported from the field (*e.g.*, FR-Aur). However, in some cases, straws are also exported from the field (*e.g*., FR-Lam). From the perspective of regional-scale applications, this term ($straw_{exp}$) is estimated as a function of the total straw biomass ($straw_{tot}$), which corresponds to the final aboveground biomass (DAM_{max}) minus the final grain yield [eq.11.3]. The sc parameter [eq.11.3.1] is estimated from in situ data during the 2011 field campaign and set to 0.3.

$$NECB = NEP + C_{exp} - C_{inp} \quad (11)$$

$$NEP = \int_{1^{st}Oct}^{30^{th}Sept} NEE \quad (11.1)$$

$$C_{exp} = Yield * C_{veg} \quad (11.2)$$

$$C_{exp} = C_{veg} * (Yield + (DAM_{max} - Yield) * sc) \quad (11.3)$$

$$sc = \frac{straw_{exp}}{straw_{tot}} = \frac{straw_{exp}}{DAM_{max} - Yield} \quad (11.3.1)$$

3.4. Model implementation and validation strategy

The proposed approach requires several types of input data, which are taken into account at different stages of the modelling process or during the calculation of the carbon budgets. To run the model, meteorological data (R_g and T_{air}), soil parameters (heterotrophic respiration parameters) and plant parameters (some being fixed and some being calibrated (see Table 2 to 6 for more details) are needed. The model can simulate the output variables only with those information, however, in the absence of calibration process, the estimates are very likely to be erroneous. To correctly simulate the crop development and thus get meaningful outputs, the satellite derived GAI is used to calibrate Pl_a, Pl_b, Sen_a, Sen_b, $ELUE_a$, SLA and D_o. Once the calibration process achieved, the parameters are set for each field and climatic year allowing to reproduce the vegetation dynamic (GAI, DAM, YLD) as well as the CO_2 fluxes (GPP, R_{eco}, NEE). Because at this stage, only remote sensing data and crop maps are needed, the approach can be up-scaled easily. Nevertheless assessing carbon budgets demand additional data that are not easily available at plot scale over large areas yet. The two additional input data needed are: the amount of C imported (C_{inp}) to the plot (as seeds and eventually as organic amendments), and an information on whether straw are exported from the plot or not. These two inputs allow to estimate the NECB [eq. 11].

The validation strategy relies on different types of datasets. Concerning the GAI, the comparison of the model output with the satellite derived GAI is not really a validation since the later is used to calibrate the model but

418 rather a verification of the model's ability to reproduce vegetation dynamic. To evaluate the performances of the
419 model to simulate biomass, data from the instrumented ICOS flux sites and from the 2011 field campaign are
420 considered. For yield validation, only the results from the 2011 field campaigns are presented (covering a range
421 of values from 1.87 to 8.93 $t.ha^{-1}$) as the annual yields provided by the farmer at the two instrumented sites may
422 be averages of several fields from the farm and therefore present high uncertainties (see Béziat et al., 2009).
423 These validations are presented in section 4.1.1.
424 To evaluate the performance of the model in terms of CO_2 flux simulations we used the data from the two ICOS
425 sites (FR-Lam and FR-Aur). The use of very contrasted climatic years and management regimes at FR-Lam and
426 FR-Aur (see section 2.2.2) makes our validation approach more robust. Those results are presented in section
427 4.1.2.
428 Among the objectives of the present study, assessing annual carbon budget is the most challenging. Indeed, the
429 performances of the model to simulate both the NEP and the amount of biomass exported at harvest must be
430 quite high to compute NECB as those two terms are usually of opposite sign and partly compensate each other.
431 A small absolute error on one of those two terms will end up in a large absolute error on the NECB. Section
432 4.2.1 presents the ability of the model to reproduce the cumulated NEE, which leads to the NEP. Then sections
433 4.2.2 and 5 present and discuss, respectively, the capability of the model to assess the NECB.
434

435 # 4. RESULTS

436 ## 4.1. Evaluation of the overall model performances

437 ### *4.1.1. GAI, DAM and yield estimates*

438 Figure 5 shows an overview of the statistical performances of the model in estimating GAI and DAM by

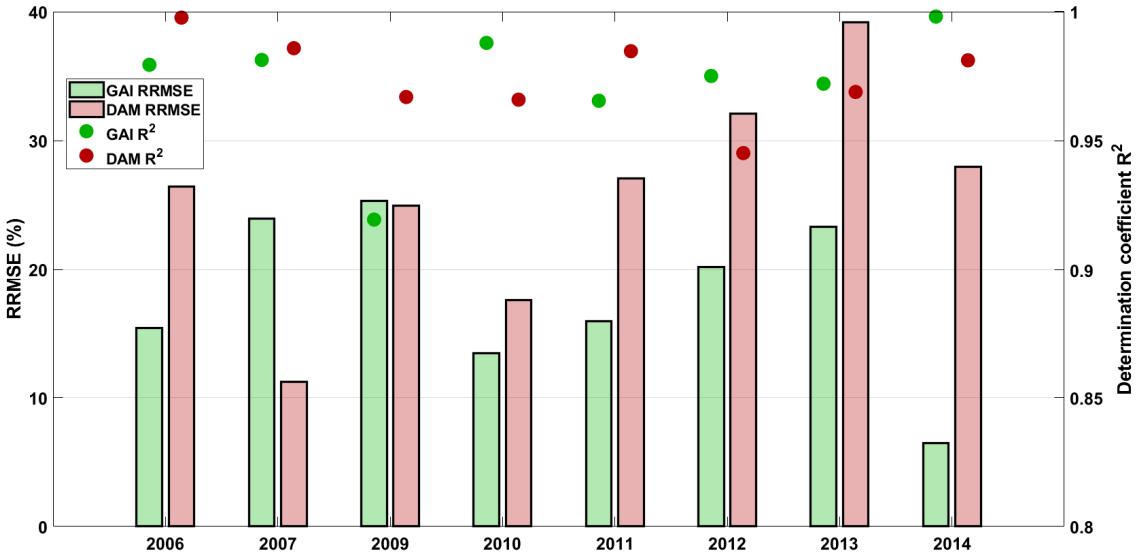

Figure 5: Statistical performances (relative root mean square errors and coefficients of determination correspond to the bars and dots, respectively) associated with the estimation of the GAI (green) and DAM (red) for winter wheat at the Auradé (even-numbered years) and Lamasquère (odd-numbered years) sites.

comparing the estimates with satellite-derived GAI and destructive biomass measurements for the FR-Aur (even-numbered years) and FR-Lam (odd-numbered years) sites in the 8 cultivation years. In addition, Figures 6a and 6b present scatter plots of these two variables, distinguishing observations performed during the entire studied period (2006-2014) at the two flux sites and measurements collected during the 2011 field campaign. At the flux sites, the GAI relative root mean square errors (RRMSEs, *i.e.,* RMSE normalized by the mean observed value) range between 6 and 24% (for the years 2014 and 2007, respectively), while the determination coefficients (R^2) are between 0.919 and 0.998 (for the years 2009 and 2014, respectively, Figure 5). When also considering fields from the 2011 campaign (Figure 6a), the GAI is reproduced by the model with a very high R^2 (0.97) and with almost no bias (0.004 $m^2.m^{-2}$). The magnitude of this performance confirms that the model allows the correct interpolation of the GAI derived from remote sensing, as has already been demonstrated in previous studies (Duchemin et al., 2015; Fieuzal et al., 2011; Hadria et al., 2010).

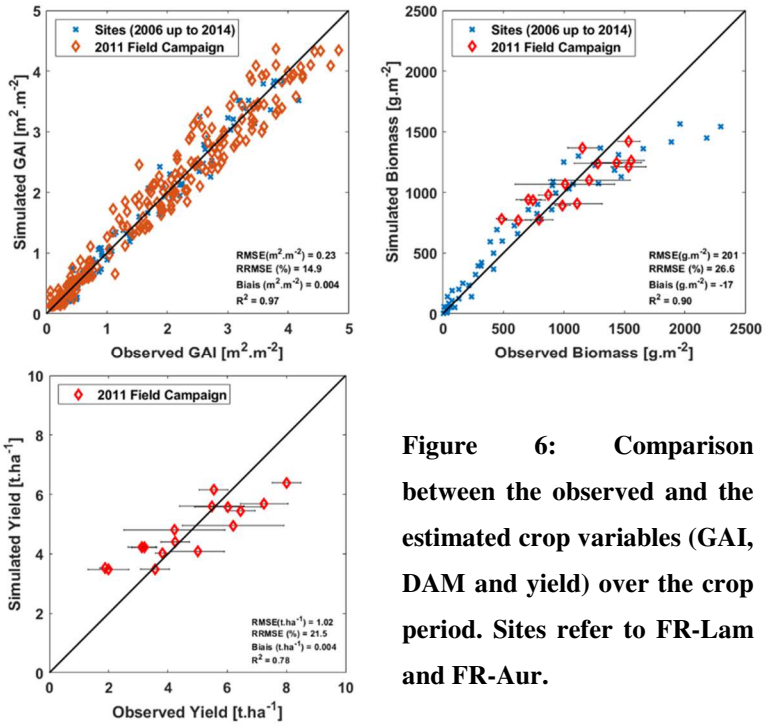

Figure 6: Comparison between the observed and the estimated crop variables (GAI, DAM and yield) over the crop period. Sites refer to FR-Lam and FR-Aur.

On average, the model also reproduces the DAM with good precision. When considering all investigated fields across the studied years (Figure 6b), the RMSE, RRMSE and R^2 were 201 $g.m^{-2}$, 26.6% and 0.90, respectively. These performances are consistent with those achieved using the SAFY model (maize and sunflower had RMSEs of 252 and 145 $g.m^{-2}$, respectively, and RRMSEs of 24.7 and 39.1%, respectively, in Claverie et al., 2012), as well as the performances of other models such as the APSIM-wheat model (Asseng et al., 1998) and STICS (Brisson et al., 2002), which estimated winter wheat biomass with R^2 of 0.90 and 0.78, respectively, and RMSEs of 0.101 and 0.266 $kg.m^{-2}$, respectively. Nevertheless, the performances are more scattered when analysing annual statistics (Figure 5). Indeed, the DAM RRMSE values are between 11 and 39.2% (for the years 2007 and 2013, respectively), while the R^2 values are between 0.945 and 0.998 (for the years 2012 and 2006, respectively). In general, the modelling approach tends to underestimate the highest biomass values at the end of the season (observed at LAM2011, AUR2012, LAM2013 and AUR2014). The highest levels of errors, for the DAM in 2012 and 2013, correspond to the strongest vegetation developments of 1960 $g.m^{-2}$ and 2298 $g.m^{-2}$, respectively, reached at the end of the crop season. Those DAM underestimations are caused by the underestimation of the effective GAI produced by BV-NNET for the highest values since the clumping effect is not accounted for (Claverie et al., 2012). This issue will be further discussed in Section 5.2.

On average, yields (only data from the 2011 field campaign are analysed here, see 2.2.1) are estimated with good

precision (RMSE=1.02 t.ha^{-1}, RRMSE=21.5%, R^2=0.78), but underestimations are observed for the highest observed values. These underestimations are directly related to the DAM underestimations described above, as yield is estimated as a fraction of the final biomass. Nevertheless, the yield-estimation performances of SAFY-CO_2 are similar to those of SAFY (Duchemin et al., 2008) and STICS (Brisson et al., 2002) for wheat, with R^2 values of 0.64 and 0.65, respectively, and RMSEs of 0.5 and 1.6 t.ha^{-1}, respectively.

4.1.2. Components of the net CO_2 fluxes: daily GPP, R_{eco} and NEE

In this section, the components of the net CO_2 fluxes simulated by SAFY-CO_2 are compared to the measured NEE at the FR-Aur and FR-Lam flux sites and with the GPP and R_{eco} estimated following the partitioning of NEE. For the 8 investigated cropping years, the model performances are evaluated in terms of the error (RMSE) and correlation (R^2) (see Figure 7). These statistical parameters are also calculated for the following periods of each cropping year (see Figure 8):

1- From the beginning of the cropping year (October 1st) until the emergence of the crop
2- From the emergence of the crop until the maximum vegetation
3- From the maximum vegetation until harvest
4- From harvest until the end of the cropping year (September 30th)

4.1.2.1 GPP estimates

When considering the whole vegetative periods (*i.e.*, crop development and post-harvest vegetative events) of the 8 site-years, the simulated GPP dynamics agree well with the measurements, showing R^2 values between 0.82 (LAM2011) and 0.94 (LAM2007) and RMSEs between 1.34 (LAM2009) and 2.39 (LAM2011) gC.m^{-2}.d^{-1}. In 2011, however, the simulated GPP during crop development showed poor statistics. A strong development of

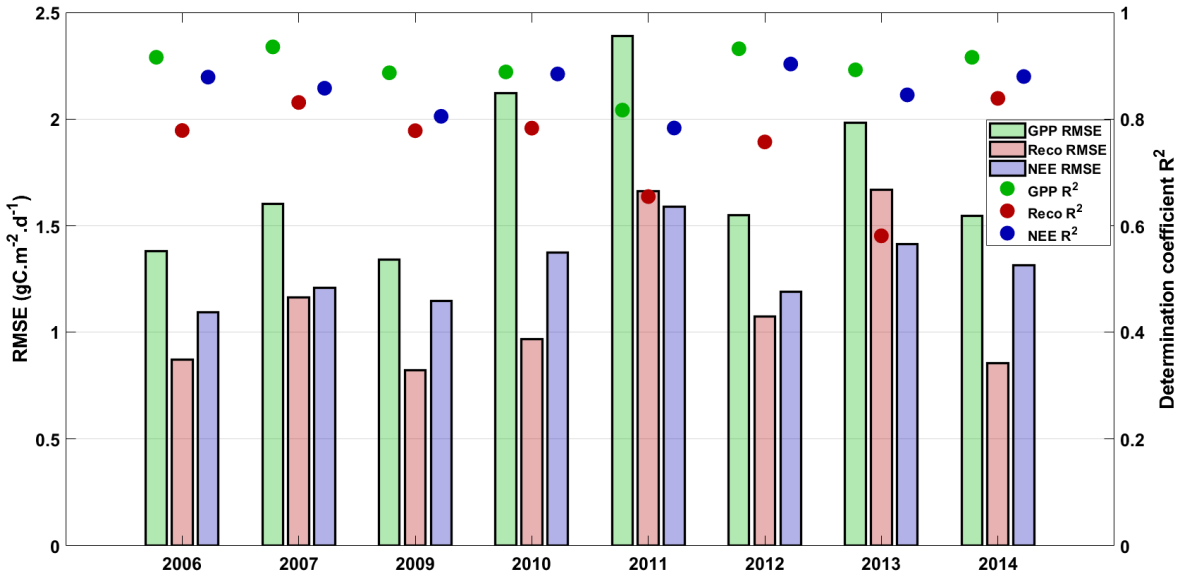

Figure 7: Statistical performances (root mean square errors and coefficients of determination are bars and dots, respectively) associated with the estimations of the daily GPP, R_{eco} and NEE for the 8 winter wheat cropping years (October 1st to September 30th) at FR-Aur (even-numbered years) and FR-Lam (odd-numbered years).

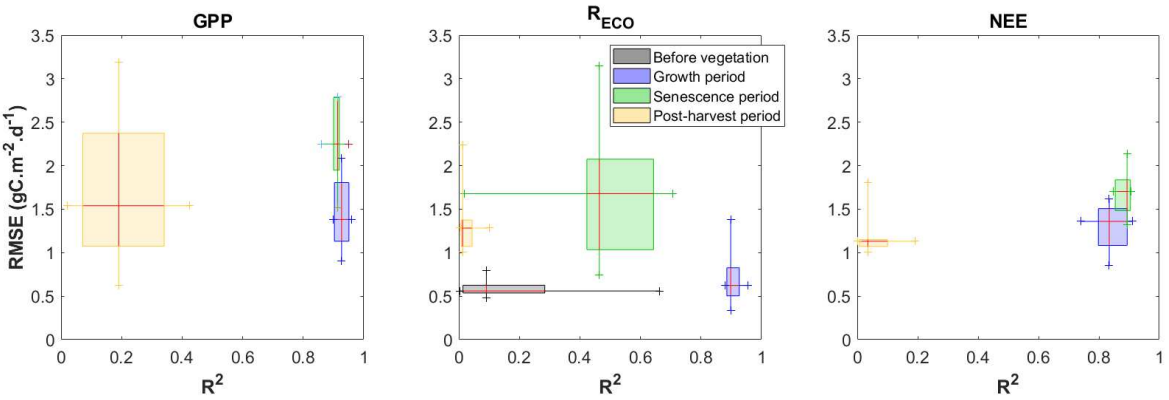

Figure 8: Boxplot of the pluriannual determination coefficients (R^2) and the pluriannual root mean square errors (RMSEs) of the simulated GPP, R_{eco} and NEE in the before-crop, crop-growth, crop-senescence, and post-harvest periods for the 8 cropping years of winter wheat at AUR and LAM. Only the years with post-harvest vegetative events (2006-2009-2011-2013) are considered for the boxplot of the post-harvest GPP.

vegetation occurred in early 2011, while no flux data were recorded between January 1st and March 31th. Consequently, the CO_2 fluxes were gap filled, and thus, the simulated GPP is underestimated over this period, leading to low R^2 and high RMSE values.

During crop development (growth and senescence, excluding post-harvest vegetative events), the simulated GPP shows R^2 values between 0.86 and 0.96 and RMSE values between 0.90 and 2.79 $gC.m^{-2}.d^{-1}$. These periods are well reproduced by the model, the growth period shows slightly better performances than the senescence period. This trend can be explained by two phenomena: i) the underestimation of the simulated GPP during senescence due to the abovementioned limits of remote-sensed GAI (underestimation due to saturation effects) coupled with the potential lack of remote sensing observations, which prevents the correct reproduction of GPP during the senescence phase and ii) the presence of weeds growing inside the senescent crop (the understorey vegetation often observed at FR-Lam), which are undetectable by the satellite but still impact the flux measurements (see *Temporal Evolution* of LAM2013 in section 4.1.2).

Considering the post-harvest period, only site-years with significant vegetative events are considered (*i.e.,* weeds for AUR2006 and LAM2009, spontaneous crop re-growth for LAM2011 and cover crops for LAM2013). The values of the R^2 between the simulated and observed GPP are lower during this period than during the crop development period for several reasons. First, at this stage, the same parameterization as the winter wheat parameterization is used for simulating the different types of post-harvest vegetative events (except concerning the parameters calibrated based on GAI satellite estimates – see section 3.2). Second the post-harvest vegetation is characterized be higher spatial heterogeneity than winter wheat, leading to likely divergence between observed and simulated CO_2 fluxes. Indeed the footprint of the EC system is probably not fully representative of the entire field simulated by the model. Nevertheless, the overall performances of the model always increase when post-harvest vegetative event are considered.

4.1.2.2 Reco estimates

Overall, the ecosystem respiration follows the same dynamics as the GPP but in an attenuated way (*i.e.,* the

differences between bare-soil and vegetative periods are smaller). The simulated R_{eco} dynamics are in good agreement with the observations, as shown in Figure 7. The annual RMSE values range from 0.82 (LAM2009) to 1.67 (LAM2013) $gC.m^{-2}.d^{-1}$, and the R^2 values range from 0.58 (LAM2013) to 0.84 (LAM2014).

The mean annual performances of the model in estimating R_{eco} are lower than those in estimating GPP but are consistent with other studies that aim to estimate ecosystem respiration in agricultural fields. Zhan et al. (2019) found R^2 values between 0.84 and 0.87 and RMSEs between 1.52 and 1.65 $gC.m^{-2}.d^{-1}$ for a maize-soybean system, while Lohila et al., (2003) estimated the total ecosystem respiration of barley with a simple soil temperature-dependent model with good precision (R^2 between 0.71 and 0.79). A more detailed analysis of our results shows that the R_{eco} is always well estimated during the crop growing periods, showing R^2 values between 0.88 and 0.95, while the statistical performances are lower in other periods than in the crop growing period (Figure 8). One explanation for this difference is that the formulation for estimating heterotrophic respiration is too simplistic to reproduce some of the processes occurring in the soil, especially after harvest. This issue will be further discussed in Section 5.2.

Additionally, for GPP, the presence of weeds growing inside the senescent crop, which is hardly detectable by the considered satellite but still impacts flux measurements (see the temporal evolution of LAM2013 in section 4.1.2.4), cannot be considered in our modelling approach. On the other hand, the good performances during the crop growing periods indicate that the model accurately reproduces autotrophic respiration, which can represent 80% of the R_{eco} during the crop season (Béziat, 2009). The modelled R_{eco} estimates are thus satisfactory considering the simplicity of its representation as well as the limited number of inputs in this crop modelling approach.

4.1.2.3 NEE estimates

The daily dynamics of the NEE are well reproduced by the SAFY-CO_2 model even when GPP and R_{eco} are underestimated, since the errors of the two components compensate for each other (either because the partitioning process overestimates the in situ data or because the model underestimates the crop development, which affects both GPP and R_{eco}). The model that shows good performances over the cropping year in terms of errors and correlations, with RMSEs between 1.09 (AUR2006) and 1.59 (LAM2011) $gC.m^{-2}.d^{-1}$ and R^2 values between 0.78 (LAM2011) and 0.90 (AUR2012). The model achieves better performances during the vegetative stages than during fallow periods (as is the case for GPP and R_{eco} due to the reasons mentioned above).

In order to compare the performances of SAFY-CO_2 to simulate NEE with other agronomical or land surface models, our results were confronted to those presented by Wattenbach et al., (2010). In their study, they compared the performances of DNDC (Li et al., 2005, 1994, 1992), ORCHIDEE-STICS (de Noblet-Ducoudré et al., 2004; Gervois et al., 2008), SPA (Williams et al., 1996) and CERES-EGC (Gabrielle et al., 2006; Lehuger et al., 2009) in reproducing the GPP, R_{eco} and NEE for several site-years, including the AUR2006 crop season. SPA and SAFY-CO_2 outperformed the other approaches by reproducing the dynamics of the cumulated NEE, with R^2 values of 0.993 and 0.995, respectively. In terms of errors, SAFY-CO_2 and CERES-EGC showed the lowest RMSEs, 33.6 $gC.m^{-2}$ and 44.16 $gC.m^{-2}$, respectively.

4.1.2.4 Temporal evolution

We decided to show the performances of SAFY-CO_2 in simulating the time courses of the GPP, R_{eco} and NEE for three contrasting site-years (AUR2006, LAM2009 and LAM2013) among the eight cultivation years. The

objectives here are i) to identify potential sources of errors in the GPP and R_{eco} estimates that can affect the NEE and the net annual CO_2 fluxes (NEP) and therefore the NECB estimates, ii) to verify whether the proposed approach is robust for varying soils, management practices and climatic years and iii) to analyse the potential of this approach to simulate contrasting post-harvest vegetative events.

- Auradé 2006

The 2006 cropping year at FR-Aur (grain farm) is characterized by very clear sky conditions and strong radiation, little precipitation in spring (23.4, 29.7 and 32.8 mm of rain during April, May and June, respectively, in 2006; in contrast, the monthly means in these months over the 8 years of the study and both sites are 64.1, 61.1 and 95.4 mm, respectively) and several re-growth/weed events occurring after harvest. For this site-year (Figure 9a), the model correctly reproduces the GPP and the R_{eco} in terms of errors (RMSEs of 1.38 and 0.87 $gC.m^{-2}.d^{-1}$, respectively) and dynamics (R^2 of 0.92 and 0.78, respectively). Consequently, the NEE for this year is accurately estimated (RMSE and R^2 of 1.09 and 0.88, respectively). Nevertheless, the modelled GPP is slightly overestimated after maximum development and at the beginning of senescence (Figure 9a). This overestimation could be related to the water stress conditions observed after the maximum GAI was reached (Béziat et al., 2013) that cannot be fully considered by the model. Moreover, spontaneous re-growth and weeds developed twice after harvest. The first event led to increases in the observed GPP and R_{eco} just after harvest and was interrupted by soil work on July 31. The second vegetative event occurred from mid-August until late September 2006 and was interrupted by soil work on September 29. In a first attempt, we simulate only one vegetation cycle after harvest, so the two events are simulated as one (see red dashed line in Figure 9a); as a consequence, GPP and R_{eco} are overestimated. NEE estimates during this period are improved (RMSE from 1.22 to 0.93 $gC.m^{-2}.d^{-1}$) by accounting for weed/re-growth development.

- Lamasquère 2009

The 2008-2009 cropping season at FR-Lam (milk and chicken production farm) was characterized by strong rains in November and December that saturated the soil, causing poor emergence and late winter wheat development. Additionally, weeds developed before harvest during the winter wheat senescence. The GPP dynamics for LAM2009 are well reproduced, with an R^2 of 0.89. Additionally, R_{eco} and NEE present R^2 values of 0.78 and 0.81, respectively, over the cultivation year. The errors of the GPP, R_{eco} and NEE are also low, showing RMSE values of 1.34, 0.82 and 1.14 $gC.m^{-2}.d^{-1}$, respectively. However, during May 4, peaks are observed in measurements (13 days in total) that are not reproduced by the model. This divergence between simulated and observed GPP comes from the underestimation of the fELUE for days with high radiation and very clear sky conditions. After harvest (from mid-July to mid-September), the presence of weeds in the field is highlighted by the measured GPP dynamics. As for 2006, the dynamics and the range of the simulated post-harvest GPP and R_{eco} are not correctly reproduced by the model since the parameterization is the same as that for winter wheat, and many phenomena are not considered (*i.e.,* priming effect, nitrogen or water stress, etc.). Nevertheless, accounting for weeds in the model allows a better estimation of the NEE (RMSEs decreasing from 1.7 to 1.14 $gC.m^{-2}.d^{-1}$).

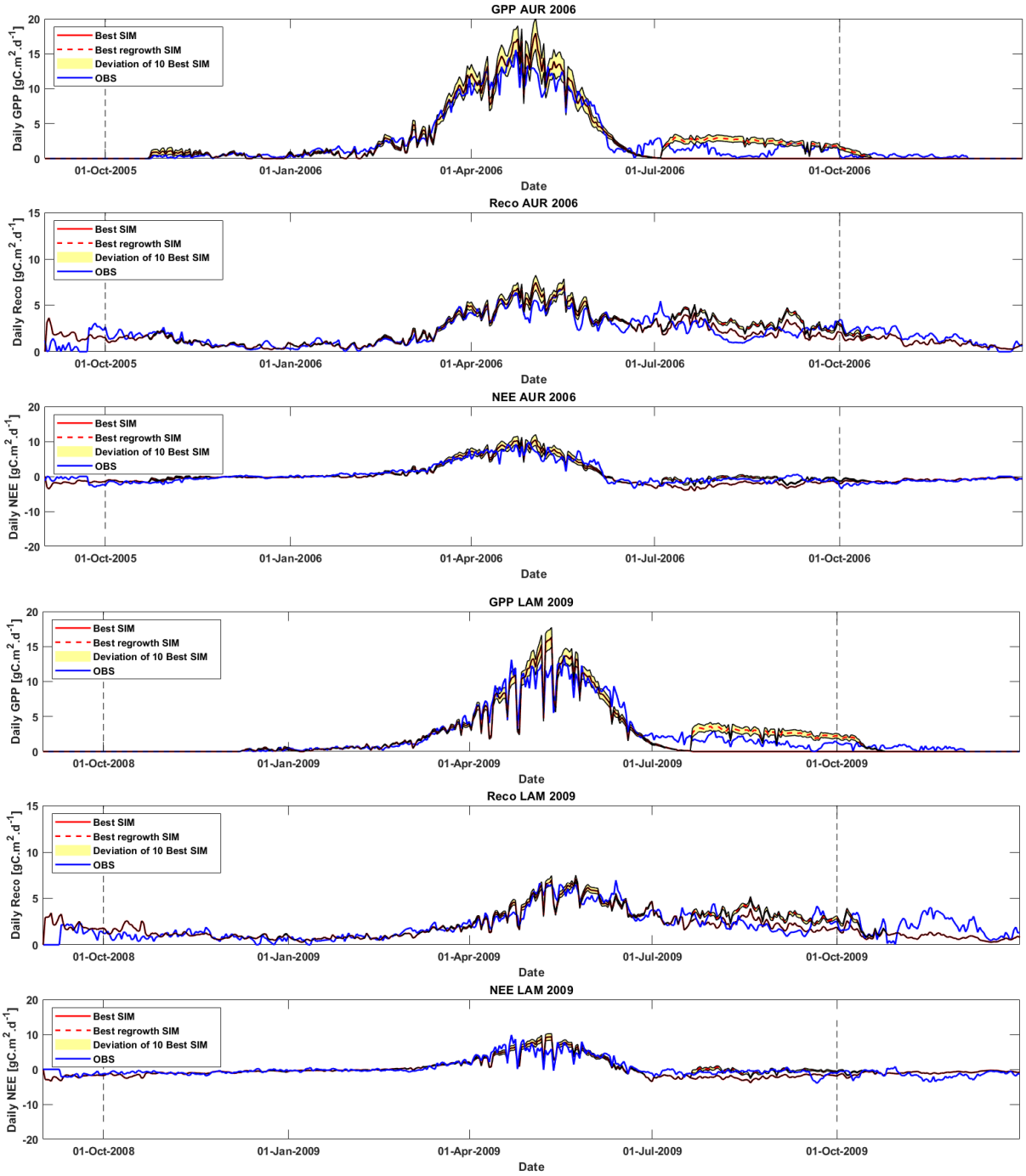

Figure 9a: Temporal evolution of the measured (in blue) and estimated (in red or red dashed lines) GPP, R_{eco} and NEE for 2 site-years (AUR2006 and LAM2009). The red/red dashed lines represent the simulations that do/do not account for re-growth and weed events. The yellow envelopes represent the daily standard deviation of the 10 (/30) best simulations (i.e. smaller RMSE GAI error). The vertical dashed lines define the cropping year.

- Lamasquère 2013

We present the results of FR-Lam over the LAM2013 cropping year because it is the only site-year during which a cover crop was grown. Indeed, in 2013 at FR-Lam, after the harvest of the winter wheat, white mustard was sown on the 21st of August and incorporated in the soil on the 4th of December. Unlike re-growth and weed development, the development of the cover crop is rather homogeneous in the field and follows a growing cycle

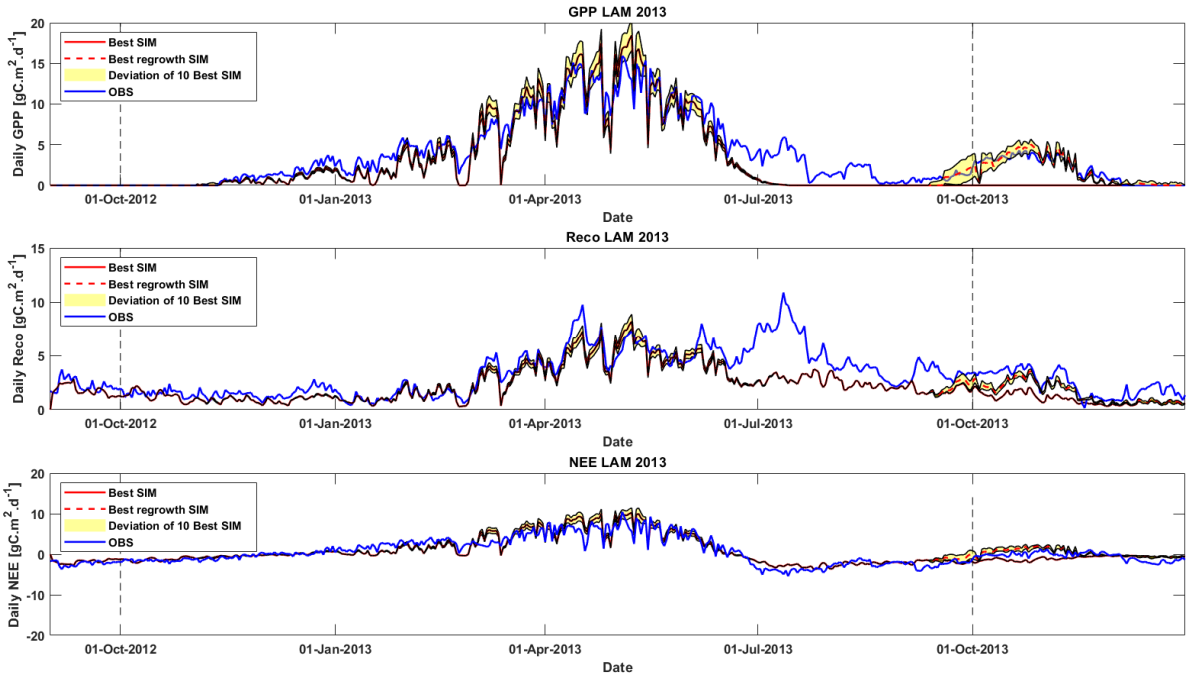

Figure 9b: Temporal evolution of the measured (in blue) and estimated (in red or red dashed lines) cumulated GPP, R_{eco} and NEE for LAM2013. The red/red dashed lines represent the simulations that do/do not account for the cover crop. The yellow envelopes represent the daily standard deviation of the 10 (/30) best simulations (i.e. smaller RMSE GAI error). The vertical dashed lines define the cropping year.

that is correctly reproduced by the model, in addition to the CO_2 fluxes (RMSE = 0.68 $gC.m^{-2}.d^{-1}$ and R^2 = 0.88 for GPP; RMSE = 1.14 $gC.m^{-2}.d^{-1}$ and R^2 = 0.62 for NEE).

LAM2013 is also marked by an early winter wheat development that benefited from good climatic and soil conditions for emergence. Therefore, the final biomass is high (2298 $g.m^{-2}$) compared to that of other years (mean and standard deviation over the 8 studied years: 1566 +/- 453 $g.m^{-2}$). This site-year is also characterized by weeds that developed during the senescence of winter wheat. These weeds could not be observed by the considered satellites, and the model was not able to simulate their effects on the CO_2 fluxes (particularly on the GPP and the R_{eco}) observed just before and after harvest. The difference between the observed and simulated NEE dynamics is small, either because the "observed" GPP and R_{eco} partly balanced each other or because the increases in the "observed" R_{eco} and GPP are caused by errors in the NEE partitioning process.

4.2. From the cumulated NEE to yearly carbon budget

4.2.1. Analysis of the cumulated NEE dynamics

For the sake of conciseness, the analysis of the temporal behaviour of the cumulated NEE focuses on the same site-years (*i.e.,* AUR2006 and LAM2009). These values are presented from October 1st until September 30th of the following year because this period corresponds to the agricultural cropping year in our area. The analysis of the cumulated NEE dynamics measured by the flux towers and modelled by SAFY-CO_2 allowed for the identification of the CO_2 net assimilation and release phases (Figure 10). A negative slope in the cumulated NEE curve (*i.e.,* corresponding to net assimilation, with GPP>R_{eco}) is observed during the growing season and during crop re-growth or weed or cover crop development. A positive slope (*i.e.,* corresponding to CO_2 release, with

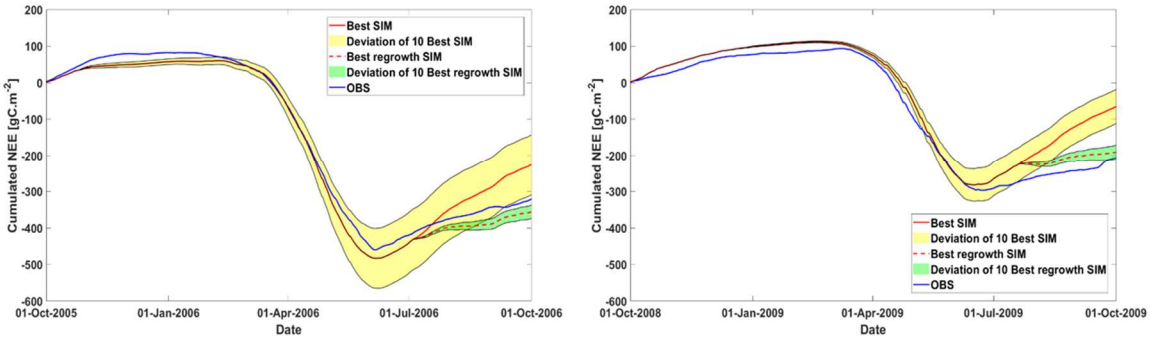

Figure 10: Temporal evolution of the measured (in blue) and estimated (in red and red dashed lines) daily values of the GPP, R_{eco} and NEE for 2 site-years: a) AUR2006 and b) LAM2009. The red/red dashed lines represent the simulations that do/do not account for re-growth and weed events. The yellow envelope represents the daily standard deviation of the 10 (/30) best simulations (i.e. smaller GAI RMSE).

GPP<R_{eco}) is observed during the bare-soil periods and the senescence stages.

The modelled cumulated NEE for AUR2006 slightly diverges from the observations before the growing season because of the underestimation of the simulated R_{eco} during this period. The effect of the overestimation of the GPP at the end of the growing stage and beginning of the senescence stage (as discussed above) leads to an underestimation of the maximum simulated cumulated NEE value.

Finally, the slope becomes positive after harvest (when there is no more GPP). The modelled cumulated NEE is well estimated when re-growth and weeds considered (red dashed line) and diverges when they are not considered in the model (red solid line).

In 2009, the simulated cumulated NEE matches well with the observations before and during the vegetative period. Indeed, over this period, the model reproduces the GPP and the R_{eco} well, leading to a good estimation of the NEE. After harvest, not considering weeds causes the model to diverge from the observations, as in 2006, while modelling post-harvest vegetation development attenuates this bias (even if the simulated weed growth starts later here than on the field).

When the post-harvest vegetative events are simulated, the difference between the observed and the simulated NEP is improved from 95 and 140 gC.m^{-2} to 33 and 16 gC.m^{-2} for AUR2006 and LAM2009, respectively.

These results emphasize the need to include the effects of re-growth events, weeds and cover crops in the model because they represent non-negligible contributions to the NEP, which in turn could have an important impact on the final annual NECB values.

4.2.2. *Carbon budget over 8 agricultural seasons of winter wheat*

The NECB model estimates and its components (NEP, C_{exp}) are compared with those of the eight site-year measurements (Table 7). In this table, the effects of post-harvest vegetative events on NEE and NECB are considered. For FR-Lam, the C_{inp} is prescribed for the calculation of the modelled NECB, as the amount of C input as organic manure cannot be estimated by remote sensing. Also, C_{inp} corresponding to the amount of seeds brought to the plots are prescribed for both sites (even if very small compared to the other terms). The NEP values estimated by SAFY-CO_2, which vary from -191 gC.m^{-2}.yr^{-1} (LAM2009) to -486 gC.m^{-2}.yr^{-1} (LAM2011), are generally close to the measured values, which vary from -208 gC.m^{-2}.yr^{-1} (LAM2009) to -410 gC.m^{-2}.yr^{-1}

(LAM2011). Table 7 shows that for all site-years, winter wheat is a CO_2 sink, and the model is able to reproduce the inter-annual variability in this sink activity. The years showing the largest difference in terms of NEP are AUR2014, AUR2012 and LAM2013, with differences of 30%, 24% and 22%, respectively, compared to observations. For AUR2014, this difference can be explained in different ways. First, the senescent phase is not well reproduced by the model because only one satellite image was available during this period, leading to an overestimation of the GPP. Second, after harvest, an increase in R_h is observed and is not reproduced by the model. This is due to the incorporation of straw into the soil, which leads to an increase in the soil microbial activity. The difference observed for AUR2012 is partly due to two post-harvest increases in R_h (priming effect) that could not be reproduced by the model. The first event, occurring at the beginning of July, was induced by rainfall. The second event followed ploughing that occurred at the beginning of August. Moreover, the NEP values of two of the three site-years where significant re-growth vegetative events occurred (during the cultural year) are better estimated once the re-growth is considered. Indeed, for AUR2006 and LAM2009, the differences between the simulated and observed NEP values are -30 and -68%, respectively, before taking re-growth into account and +10 and -7.8%, respectively, after taking re-growth into account. For LAM2011, NEP is first underestimated (-21%) and then overestimated (+19%).

The analysis of the amount of carbon exported from the ecosystem at harvest (C_{exp}) shows that this amount varies considerably from one site-year to another. The simulated C_{exp} varies from 253 $gC.m^{-2}.yr^{-1}$ (AUR2010) to 436 $gC.m^{-2}.yr^{-1}$ (LAM2013), while the observations range from 204 $gC.m^{-2}.yr^{-1}$ (AUR2010) to 488 $gC.m^{-2}.yr^{-1}$ (LAM2013). C_{exp} values are often larger at FR-Lam than at FR-Aur due to the export of grain and straw and the model tends to overestimate the C_{exp}. The differences between the observations and model estimates of C_{exp} vary between 5% and 46%. However, the comparison of the modelled C_{exp} and the observed C_{exp} should be performed with caution since the precision of the yield provided by the farmer is questionable (especially at the Lamasquère site where most of the straws are exported) since those values are averaged over several fields of the farm (see section 2.2.1.). For this reason, Béziat et al. (2009) concluded that the uncertainty of in situ C_{exp} is often higher than the uncertainty of the NEP at our sites. For AUR2012, for instance, the C_{exp} estimated from the farmer's data is 223 $gC.m^{-2}.yr^{-1}$, while our destructive measurements encompassing over 30 subplots of $3.75*10^{-2}$ m^2 in the field suggest a C_{exp} of 406+/-53 $gC.m^{-2}.yr^{-1}$. When analysing the performance of the model against our own destructive field samples, the model generally performs much better (see Figure 6b and 6c). This indicates that our modelling approach may perform better for estimating C_{exp} (and therefore NECB) than what is presented in

Site-Year	NEP				Cinp	Cexp				NECB			
	SIM	OBS [gC/m²/yr]	Diff	Diff [%]	OBS [gC/m²/yr]	SIM	OBS [gC/m²/yr]	Diff	Diff [%]	SIM	OBS [gC/m²/yr]	Diff	Diff [%]
AUR2006	-355	-322 ± 20	-33	10	-6.25 ± 1.88	270	216 ± 56	54	25	-94	-113 ± 60	19	-17
LAM2007	-302	-371 ± 33	69	-19	-389 ± 95.4	387	322 ± 29	65	20	-304	-439 ± 105	135	-31
LAM2009	-191	-208 ± 19	17	-8	-150 ± 45	293	279 ± 25	14	5	-48	-78 ± 55	30	-38
AUR2010	-253	-301 ± 47	48	-16	-6.25 ± 1.88	253	204 ± 53	49	24	-6	-102 ± 71	96	-94
LAM2011	-486	-410 ± 45	-76	19	-166 ± 49.8	400	355 ± 32	45	13	-252	-221 ± 74	-31	14
AUR2012	-362	-293 ± 34	-69	24	-6.25 ± 1.88	326	223 ± 20	103	46	-41	-76 ± 40	35	-46
LAM2013	-421	-345 ± 32	-76	22	-178 ± 53.4	436	488 ± 40	-52	-11	-163	-36 ± 74	-127	355
AUR2014	-316	-243 ± 34	-73	30	-6.25 ± 1.88	285	214 ± 67	71	33	-31	-29 ± 75	-2	6
SIM vs. OBS All Sites	**RMSE [gC/m²/yr]**		61		-	**RMSE [gC/m²/yr]**		61		**RMSE [gC/m²/yr]**		77	
	RMSE [%]		-19.7			**RMSE [%]**		21.3		**RMSE [%]**		-56.1	
	R²		0.58			**R²**		0.83		**R²**		0.66	

Table 7: Annual net ecosystem carbon budgets (NECB) and their components (NEP, Cinp, Cexp) derived from the in-situ (OBS) and modelled (SIM) data for 8 site-years. Uncertainties on observations are also shown (for more details see Béziat et al., 2009).

Table 7.

The NECB estimated from in situ data or from SAFY-CO_2 characterize all of the site-years as carbon sinks. The modelled NECB estimates vary from -304 $gC.m^{-2}.yr^{-1}$ (LAM2007) to -6 $gC.m^{-2}.yr^{-1}$ (AUR2010), while the in situ NECB estimates vary from -439 $gC.m^{-2}.yr^{-1}$ (LAM2007) to -29 $gC.m^{-2}.yr^{-1}$ (AUR2014). The FR-Lam site-years present the greatest variations between years, and the carbon inputs (NEP + C_{inp}) are stronger than those of FR-Aur, partly because of organic fertilization.

As shown in Table 7, the relative differences between the modelled and in-situ NECB vary from 6% (AUR2014) to 355% (LAM2013). In absolute terms, these differences vary from 2 $gC.m^{-2}.yr^{-1}$ (AUR2014) to 135 $gC.m^{-2}.yr^{-1}$ (LAM2007) but the sign of NECB is always similar between both approaches. Regarding all simulated years, the model shows RMSE of 77 $gC.m^{-2}.yr^{-1}$. Note however that, the modelled NECB match to that observed for five simulated years out of eight if the uncertainties are considered. Indeed, the uncertainties on the in-situ NECBs (derived from uncertainties on the observed NEP, C_{inp}, C_{exp}) range from 40 to 105 $gC.m^{-2}.d^{-1}$. These results highlight the importance of precisely estimating each of the terms that compose the NECB to obtain accurate estimations of the annual crop carbon budgets (both with the in-situ and the modelling approaches).

5. DISCUSSION

5.1. Performances and benefits of our approach

In this study, our objective is to evaluate the potential of high resolution GAI products assimilation into a simple crop model for simulating the biomass, the yield, the net CO_2 fluxes components and the annual C budget of winter wheat crops at plot scale. The main advantage of this approach is that it requires few input data and little or no external information about management practices. Also, even with a limited number of equations and parameters compared to more complex crop models that require data on management practices, SAFY-CO_2 achieves equivalent or better performances regarding estimates of key components of the C budget: CO_2 fluxes, biomass and yield (see sections 4.1.1. and 4.1.2.).

Next, we demonstrated the ability of the model to reproduce winter wheat dynamics, production and CO_2 fluxes under contrasted climatic and management conditions with the same parametrization. It shows the ability of such a remote sensing driven diagnostic approach (*e.g.* for calculating GPP) to account implicitly for the main stresses (N, drought, temperature…) and the main crop development limiting factors.

Finally, our methodology allows accounting for the effect of post-harvest spontaneous re-growth, weeds and cover crops on the CO_2 fluxes. As showed by Ceschia et al., (2010) this is essential for estimating accurately cropland C budgets and only remote sensing based approaches allow characterizing the dynamics and the spatial heterogeneity of the various post-harvest vegetative events. Therefore, in spite of a generic parameterization of the SAFY-CO_2 model for those post-harvest vegetative events, the overall performances of the model for simulating CO_2 fluxes and C budgets always increase when they are accounted for. The performances should improve thanks to the higher temporal resolution of the Sentinel missions. Next step could be to apply a specific parametrization, depending on the nature of those events or on their species composition (*e.g.* for cover crops), provided that the information is given by the farmer or can be retrieved by remote sensing (*e.g.* through cover crop classification).

5.2. Potential limitations of this approach and drawbacks for large scale application

The first main limitation of this approach based on optical remote sensing is that gaps in optical remote sensing observations during crucial periods of the crop development could lead to wrong estimates of the GAI dynamics, biomass and CO_2 fluxes or could even make our approach inoperative (*e.g.* in 2007-2008). Fortunately, recent Sentinel 2 satellite missions provide observations at high spatial resolution (10m) every 5 days all over the globe which could partially solve this problem. Also, it was shown that the combined use of optical and Synthetic Aperture Radar (SAR) satellite data, like Sentinel 1, can overcome this issue (see Ameline et al., 2018; Baup et al., 2019; Betbeder et al., 2016; Remy Fieuzal et al., 2017; Revill et al., 2013). Indeed, the signal of the SAR satellites is not affected by clouds and they can even observe the surface at night. Another limitation of this optical remote sensing approach is that it cannot detect understorey vegetation (*e.g.* weeds) and their effect on the CO_2 fluxes. Here again SAR data may overcome this issue as microwave signal are associated to deeper penetration capabilities (compared to optical reflectance), depending on the considered wavelength, and providing a valuable information on vegetation structure and water content (Brown et al., 2003).

The second main limitation of this approach concerns the availability of plot scale information regarding straw management and organic fertilization. Those practices cannot be detected or quantified by remote sensing at this stage and therefore the uncertainty on the C budgets estimates in areas where animal farming occurs is high. This issue may be overcome in the future if data from the Farm Management Information Systems (FMIS) become more easily and more widely accessible. Another limitation for applying our approach concerns the size and the shape of the agricultural plots. As mentioned above, the contours of the plots must be eroded so that the signal is not influenced by surrounding landscape elements. Thus, we consider that for plots below 0.5-1 ha, GAI products may not be of good enough quality to apply our approach. Also high resolution GAI and crop maps are needed in our approach. In Europe, the later can be obtained via the Land Parcel Identification System (LPIS) and both data inputs should be available in a near future via the High Resolution Layers Copernicus Land Monitoring Service (https://land.copernicus.eu/pan-european/high-resolution-layers). The last limitation of our approach is that it cannot be used for forecasting, since it is based on satellite observations, although it is possible to test the effect of some scenarii on the C budgets (*e.g.* accounting or not for the effects of the post-harvest vegetative events or for the impact of exporting or not the straw from the plot).

Of course the question of the transposability of our approach and of its domains (spatial and temporal) of validity should be considered with caution. Indeed, the current parametrization of the SAFY-CO_2 model is adapted to the pedoclimatic conditions where it has been set and it should be adapted to other crop species. Also the boundaries of the calibrated winter wheat phenological parameters are set for our pedoclimatic conditions. Applying this approach to areas where winter wheat has different periods of emergence and senescence would require to redefine those boundaries (*e.g.* in Northern countries). Note however that 1) the future High Resolution Phenology Copernicus Land Monitoring Service should provide, all over Europe since 2017, the dates of emergence and end of the growing for the crops and cover crops at plot scale for each cropping year by the end of this year and that 2) the transposability of the original SAFY model has already been tested in contrasted pedoclimatic conditions (France, Mexico and Morocco; see (Claverie et al., 2012; Duchemin et al., 2015, 2008; respectively) and for different crop species (corn, soybean, sunflower and wheat).

Also, the parametrisation of the Q_{10} based approach for estimating heterotrophic respiration is well adapted to the type of soils and climates similar to the ones found in our area of study but it should probably be adapted to

other soil types (*e.g.* organic or sandy soils) and climatic conditions. Still, with a similar approach, Delogu et al., (2017) obtained good R_h estimates (RMSE comprised between 0.15 and 0.73 $gC.m^{-2}.d^{-1}$ and R^2 between 0.42 and 0.92 depending on the site) over contrasted pedoclimatic conditions. Another potential issue concerning our approach relates to the simplistic method for estimating R_h which should be considered as a first step for estimating R_h. In the future, this method could be improved, with little changes in the formalisms, by considering a R_{10} parameter that depends on top soil slow carbon content as it is proposed in Delogu et al., (2017). Another step of improvement could be to account for the priming effect following the incorporation of fresh organic matter into the soil (Kuzyakov et al., 2000). Indeed, with our modelling approach we could already estimate the amount of crop residues, cover crop, weeds and spontaneous re-growth incorporated in the soil. However accounting for the effect of organic fertilization is not an option at this stage, since this kind of information is not yet available at plot scale over large areas. For similar reasons, we did not account for the effect of soil work on soil respiration and also because it was shown that it has no significant effect on soil respiration (Eugster et al., 2010) and no clear effect on SOC mineralisation (*e.g.* in Dimassi et al., 2014; Powlson et al., 2016; Virto et al., 2012). Also, a potential drawback of our approach for estimating R_h is that the effect of the soil water content is not accounted for. As for the SAFY model (Battude et al., 2017; Duchemin et al., 2015), we have already tested the coupling of a soil water module (FAO56; Allen et al., 1998) to the SAFY-CO_2 model (see Veloso, 2014). Such a coupling allows accounting for soil water content effects on photosynthesis and on heterotrophic respiration, and requires that accurate data concerning soil properties (*e.g.* texture, depth) at the plot scale are available. Unfortunately, the current products mapping soil properties (*e.g.* GlobalSoilMap, SoilGrids) either have a too coarse resolution for our area of study (250 m, for SoilGrids) or have too little accuracy to meet the needs of a SAFY-CO_2 – soil water module coupled approach at plot scale (*e.g.* the performances of GlobalSoilMap in France are $R^2 = 0.27$ and RMSE = 128 $g.kg^{-1}$ for clay content). Therefore, in the perspective of up-scaling our current approach for estimating annual cropland C budgets, we chose to rely only on currently available and sufficiently accurate data at plot scale. This is the reason why we chose a simple Q_{10} approach for estimating heterotrophic respiration at this stage. Of course, if this choice is likely suitable for plot scale annual C budget estimates, at crop rotation scale or over longer periods of study, the coupling of the SAFY-CO_2 model with a soil organic matter model (*e.g.* RothC, Coleman and Jenkinson, 1996; AMG, Saffih-Hdadi and Mary, 2008) should be considered. Such a step would benefit from 1) the improvement of the current soil products (*e.g.* GlobalSoilMap) which could be achieved by developing the current methods of inversion based on high resolution multi-spectral or hyperspectral remote sensing data (see Castaldi et al., 2019; Vaudour et al., 2019) and 2) from an easier and more systematic access to the FMIS data.

Another limitation of our modelling approach is that it tends to underestimate the highest biomass values at the end of the season and therefore also the yield, impacting the C budgets estimates. These underestimations may be partly due to the underestimation of satellite-derived GAI (Claverie et al., 2012). In such a context, the assimilation of both GAI derived from optical images and dry biomass estimated from SAR images into the agro-meteorological model overcomes the limitation, as presented by Betbeder et al., (2016) in the specific case of soybean. Furthermore, taking into account the clumping effect in radiative transfer model would make it possible to limit the underestimation of GAI values (derived from optical images) when vegetation becomes dense.

Still, we show that, within the limit of its domain of application, our approach was able to reproduce correctly

the GAI, biomass and CO_2 flux dynamics and it was able to estimate the NEP with a satisfactory level of accuracy. The relatively large error of prediction on the C budgets (mean RMSE of 77 $gC.m^{-2}.yr^{-1}$ and rRMSE of 56 %) has to be tempered considering the uncertainties on the NECB calculated from the in-situ data. Indeed, besides the inherent uncertainties on the NEP associated to measurements errors and data processing, there is a strong uncertainty on the in-situ C_{exp} term for the two ICOS sites as mentioned previously. Considering the resulting uncertainties on the in-situ NECB, we conclude that the modelled NECB match the observations for five years out of eight. Also, section 4.1.2.4 showed that the model was able to estimate the yield with a rather good precision, suggesting that the error on the NECB could be reduced when comparing our estimates with in-situ NECB calculated with more accurate yield data. Still, even if SAFY-CO_2 provided accurate estimations of the annual components of the NECB we cannot claim at this stage that the model can reproduce accurately carbon budgets, especially over the long term. More accurate in-situ data, a larger dataset of validation and/or simulations on longer periods evaluated against estimates of soil C stock changes based on soil analysis would be needed to conclude.

Of course other approaches allowing to estimate carbon budget exist, such as soil organic matter models which are designed to simulate the evolution of soil C stocks. The two most widely used and validated SOM are Roth-C (Coleman and Jenkinson, 1996) and CENTURY (Parton et al., 1987). Those models estimate soil C stock changes have been evaluated against long term experiments. Contrary to the proposed approach, they need information about soil texture, management practices or residue quality. Their relative error in estimating soil C stock changes is comprised between 2-30% (Falloon and Smith, 2006; Guo et al., 2007; Smith et al., 1997) for Roth-C model and between 1.8-16.4% for CENTURY (Cong et al., 2014; Falloon and Smith, 2003). These results, which are more accurate than those achieved with SAFY-CO_2 model should be tempered by the fact that they represent two different approaches, requiring different input and designed for different purposes and time-scales.

Also, as in other studies (Ceschia et al., 2010; Schmidt et al., 2012) our results showed that for all cropping years the plots behave as a net CO_2 sinks and our results concerning the potential C storage of winter wheat crop are consistent with other studies (*e.g.* Aubinet et al., 2009; Ceschia et al., 2010). In addition, our results show that, in soils with low SOC content, post-harvest vegetative events (*e.g.* cover crops) increase soil organic carbon storage which is consistent with other studies (Kaye and Quemada, 2017; Pellerin et al., 2019; Poeplau and Don, 2015; Tribouillois et al., 2018).

Finally, in spite of the limitations and potential drawbacks of this approach, it seems to be a good compromise for estimating the components of the annual C budgets over large areas at this stage and we think that it offers great perspectives of development and applications at large scale thanks to the new satellite missions and Copernicus services.

6. CONCLUSION

In this work, we demonstrate the potential of high-resolution remote sensing data assimilation in a semi-physical crop model (SAFY-CO_2) to successfully provide estimates of some of the main components of cropland annual carbon budgets (*i.e.,* net CO_2 flux components and yield). While this modelling approach is promising because it requires few input parameters and no management data for estimating crop production and net CO_2 fluxes, this approach should be considered a first step for filling the gap in obtaining spatially explicit representation of the

main components of cropland carbon budgets at the regional scale for a crop rotation or longer. Indeed, the main limitation of this approach is that, in areas concerned with animal farming, the calculation of the carbon budget requires data on i) organic amendments and ii) the fraction of straw exported at harvest, which presently cannot be retrieved by remote sensing at this stage. The second main limitation relates to the fact that the simple Q_{10} based approach for estimating heterotrophic respiration does not allow us to estimate accurately the C budget for periods longer than the cropping year. For longer periods of study, the benefit of coupling our model with a soil module should be investigated. Another limitation concerns the availability of satellite observations, since our approach is data driven. However, because of recent HTRS satellite missions (Sentinel 2 and Landsat-7&8), this type of approach could be generalized and more accurate and robust. Synthetic aperture radar satellites (*e.g.*, Sentinel 1) could also be used to overcome cloudy conditions (Veloso et al., 2017). In addition, our results show that the performance of the model in estimating net CO_2 fluxes and thus C budgets are significantly improved by considering the development of weeds and crop re-growth after harvest. These events, as well as the presence of cover crops in crop rotations, are rarely or never accounted for in regional or global modelling of CO_2 fluxes, although they significantly impact cropland carbon budgets.

In the perspective of future global-scale applications, our approach could be strengthened (validated for a wider range of climates and management regimes) and extended to other crops by using data from international flux networks (*e.g.*, ICOS and FLUXNET) and from recent HTRS satellite missions.

Acknowledgements

This work was made possible through the support of the Agence De l'Environnement et de la Maîtrise de l'Energie (ADEME), which financed the project "Couverts Intermédiaires pour l'atténuation du Changement Climatique" (CICC) and half of Gaétan's and Morgan's PhDs, the Centre National d'Etudes Spatiales (CNES), which financed half of Gaétan's PhD, and the Agence de l'Eau Adour Garonne (AEAG), which financed the Bag'ages project and the support of the European Union that financed the Sensagri project (Horizon 2020 Research and Innovation Programme, Grant Agreement n°730074).

Data acquisition at FR-Lam and FR-Aur were mainly funded by the Institut National des Sciences de l'Univers of the Centre National de la Recherche Scientifique (CNRS-INSU) through the ICOS and OSR SW observatories. Facilities and staff were also funded and supported by the University Toulouse III - Paul Sabatier, the CNES and IRD (Institut de Recherche pour le Développement). We are grateful to Franck Granouillac, Nicole Claverie, Bernard Marciel and Pascal Keravec for their technical support, advice, and valuable assistance in the field and with site management. We extend special thanks to Mr. Andréoni (farmer) and to the Ecole d'Ingénieur de Purpan for accommodating our measurement devices in their fields at FR-Aur and FR-Lam respectively.

We are also very grateful to Pauline Buysse and Benjamin Loubet (respectively Grignon's site manager and PI), Bernard Heinesch (Lonzee's PI), Nina Buchmann (Oensingen's PIs) and Christian Bernhofer (Klingenberg's PI) for granting and facilitating our access to their flux site data (destructive GAI, CO_2 flux, radiation and temperature measurement and management data), which allowed us to account for diffuse radiation effects in GPP estimates.

REFERENCES

Allen, R. G., Pereira, L. S., Raes, D., & Smith, M. (1998). Crop evapotranspiration-Guidelines for computing crop water requirements-FAO Irrigation and drainage paper 56. *Fao, Rome*, *300*(9), D05109.

Ameline, M., Fieuzal, R., Betbeder, J., Berthoumieu, J.-F., Baup, F., 2018. Estimation of Corn Yield by Assimilating SAR and Optical Time Series Into a Simplified Agro-Meteorological Model: From Diagnostic to Forecast. IEEE J. Sel. Top. Appl. Earth Obs. Remote Sens. 11, 4747–4760. https://doi.org/10.1109/JSTARS.2018.2878502

Amthor, J., 2000. The McCree–de Wit–Penning de Vries–Thornley Respiration Paradigms: 30 Years Later. Ann. Bot. 86, 1–20. https://doi.org/10.1006/anbo.2000.1175

Amthor, J.S., 1989. Respiration and Crop Productivity. Springer US, New York, NY.

Arnaud, M., Leroy, M., 1991. SPOT 4: a new generation of SPOT satellites. ISPRS J. Photogramm. Remote Sens. 46, 205–215. https://doi.org/10.1016/0924-2716(91)90054-Y

Asseng, S., Keating, B.A., Fillery, I.R.P., Gregory, P.J., Bowden, J.W., Turner, N.C., Palta, J.A., Abrecht, D.G., 1998. Performance of the APSIM-wheat model in Western Australia. Field Crops Res. 57, 163–179. https://doi.org/10.1016/S0378-4290(97)00117-2

Aubinet, M., Grelle, A., Ibrom, A., Rannik, Ü., Moncrieff, J., Foken, T., Kowalski, A.S., Martin, P.H., Berbigier, P., Bernhofer, Ch., Clement, R., Elbers, J., Granier, A., Grünwald, T., Morgenstern, K., Pilegaard, K., Rebmann, C., Snijders, W., Valentini, R., Vesala, T., 1999. Estimates of the Annual Net Carbon and Water Exchange of Forests: The EUROFLUX Methodology, in: Advances in Ecological Research. Elsevier, pp. 113–175. https://doi.org/10.1016/S0065-2504(08)60018-5

Aubinet, M., Moureaux, C., Bodson, B., Dufranne, D., Heinesch, B., Suleau, M., Vancutsem, F., Vilret, A., 2009. Carbon sequestration by a crop over a 4-year sugar beet/winter wheat/seed potato/winter wheat rotation cycle. Agric. For. Meteorol. 149, 407–418. https://doi.org/10.1016/j.agrformet.2008.09.003

Baldocchi, D.D., 2003. Assessing the eddy covariance technique for evaluating carbon dioxide exchange rates of ecosystems: past, present and future. Glob. Change Biol. 9, 479–492. https://doi.org/10.1046/j.1365-2486.2003.00629.x

Baret, F., Hagolle, O., Geiger, B., Bicheron, P., Miras, B., Huc, M., Berthelot, B., Niño, F., Weiss, M., Samain, O., Roujean, J.L., Leroy, M., 2007. LAI, fAPAR and fCover CYCLOPES global products derived from VEGETATION. Remote Sens. Environ. 110, 275–286. https://doi.org/10.1016/j.rse.2007.02.018

Baret, F., Olioso, A., Luciani, J.L., 1992. Root biomass fraction as a function of growth degree days in wheat. Plant Soil 140, 137–144. https://doi.org/10.1007/BF00012815

Battude, M., Al Bitar, A., Brut, A., Tallec, T., Huc, M., Cros, J., Weber, J.-J., Lhuissier, L., Simonneaux, V., Demarez, V., 2017. Modeling water needs and total irrigation depths of maize crop in the south west of France using high spatial and temporal resolution satellite imagery. Agric. Water Manag. 189, 123–136. https://doi.org/10.1016/j.agwat.2017.04.018

Battude, M., Al Bitar, A., Morin, D., Cros, J., Huc, M., Marais Sicre, C., Le Dantec, V., Demarez, V., 2016. Estimating maize biomass and yield over large areas using high spatial and temporal resolution Sentinel-2 like remote sensing data. Remote Sens. Environ. 184, 668–681. https://doi.org/10.1016/j.rse.2016.07.030

Baup, F., Ameline, M., Fieuzal, R., Frappart, F., Corgne, S., Berthoumieu, J.-F., 2019. Temporal Evolution of Corn Mass Production Based on Agro-Meteorological Modelling Controlled by Satellite Optical and SAR Images. Remote Sens. 11, 1978. https://doi.org/10.3390/rs11171978

Baveye, P.C., Berthelin, J., Tessier, D., Lemaire, G., 2018. The "4 per 1000" initiative: A credibility issue for the soil science community? Geoderma 309, 118–123. https://doi.org/10.1016/j.geoderma.2017.05.005

Berjón, A.J., Cachorro, V.E., Zarco-Tejada, P.J., de Frutos, A., 2013. Retrieval of biophysical vegetation parameters using simultaneous inversion of high resolution remote sensing imagery constrained by a vegetation index. Precis. Agric. 14, 541–557. https://doi.org/10.1007/s11119-013-9315-8

Betbeder, J., Fieuzal, R., Baup, F., 2016. Assimilation of LAI and Dry Biomass Data From Optical and SAR Images Into an Agro-Meteorological Model to Estimate Soybean Yield. IEEE J. Sel. Top. Appl. Earth Obs. Remote Sens. 9, 2540–2553. https://doi.org/10.1109/JSTARS.2016.2541169

Béziat, P., 2009. Effet des conditions environnementales et des pratiques culturales sur les flux de carbone et d'eau dans les agrosystèmes, Université Paul Sabatier, Toulouse III.

Béziat, P., Ceschia, E., Dedieu, G., 2009. Carbon balance of a three crop succession over two cropland sites in South West France. Agric. For. Meteorol. 149, 1628–1645. https://doi.org/10.1016/j.agrformet.2009.05.004

Béziat, P., Rivalland, V., Tallec, T., Jarosz, N., Boulet, G., Gentine, P., Ceschia, E., 2013. Evaluation of a simple approach for crop evapotranspiration partitioning and analysis of the water budget distribution for several crop species. Agric. For. Meteorol. 177, 46–56. https://doi.org/10.1016/j.agrformet.2013.03.013

Brisson, N., Mary, B., Ripoche, D., Jeuffroy, M.H., Ruget, F., Nicoullaud, B., Gate, P., Devienne-Barret, F., Antonioletti, R., Durr, C., Richard, G., Beaudoin, N., Recous, S., Tayot, X., Plenet, D., Cellier, P.,

Machet, J.-M., Meynard, J.M., Delécolle, R., 1998. STICS: a generic model for the simulation of crops and their water and nitrogen balances. I. Theory and parameterization applied to wheat and corn. Agronomie 18, 311–346. https://doi.org/10.1051/agro:19980501

Brisson, N., Ruget, F., Gate, P., Lorgeou, J., Nicoullaud, B., Tayot, X., Plenet, D., Jeuffroy, M.-H., Bouthier, A., Ripoche, D., Mary, B., Justes, E., 2002. STICS: a generic model for simulating crops and their water and nitrogen balances. II. Model validation for wheat and maize. Agronomie 22, 69–92. https://doi.org/10.1051/agro:2001005

Brown, S.C.M., Quegan, S., Morrison, K., Bennett, J.C., Cookmartin, G., 2003. High-resolution measurements of scattering in wheat canopies-implications for crop parameter retrieval. IEEE Trans. Geosci. Remote Sens. 41, 1602–1610. https://doi.org/10.1109/TGRS.2003.814132

Bsaibes, A., Courault, D., Baret, F., Weiss, M., Olioso, A., Jacob, F., Hagolle, O., Marloie, O., Bertrand, N., Desfond, V., Kzemipour, F., 2009. Albedo and LAI estimates from FORMOSAT-2 data for crop monitoring. Remote Sens. Environ. 113, 716–729. https://doi.org/10.1016/j.rse.2008.11.014

Calvet, J.-C., Noilhan, J., Roujean, J.-L., Bessemoulin, P., Cabelguenne, M., Olioso, A., Wigneron, J.-P., 1998. An interactive vegetation SVAT model tested against data from six contrasting sites. Agric. For. Meteorol. 92, 73–95. https://doi.org/10.1016/S0168-1923(98)00091-4

Castaldi, F., Hueni, A., Chabrillat, S., Ward, K., Buttafuoco, G., Bomans, B., Vreys, K., Brell, M., van Wesemael, B., 2019. Evaluating the capability of the Sentinel 2 data for soil organic carbon prediction in croplands. ISPRS J. Photogramm. Remote Sens. 147, 267–282. https://doi.org/10.1016/j.isprsjprs.2018.11.026

Ceschia, E., Béziat, P., Dejoux, J.F., Aubinet, M., Bernhofer, Ch., Bodson, B., Buchmann, N., Carrara, A., Cellier, P., Di Tommasi, P., Elbers, J.A., Eugster, W., Grünwald, T., Jacobs, C.M.J., Jans, W.W.P., Jones, M., Kutsch, W., Lanigan, G., Magliulo, E., Marloie, O., Moors, E.J., Moureaux, C., Olioso, A., Osborne, B., Sanz, M.J., Saunders, M., Smith, P., Soegaard, H., Wattenbach, M., 2010. Management effects on net ecosystem carbon and GHG budgets at European crop sites. Agric. Ecosyst. Environ. 139, 363–383. https://doi.org/10.1016/j.agee.2010.09.020

Chabbi, A., Lehmann, J., Ciais, P., Loescher, H.W., Cotrufo, M.F., Don, A., SanClements, M., Schipper, L., Six, J., Smith, P., Rumpel, C., 2017. Aligning agriculture and climate policy. Nat. Clim. Change 7, 307–309. https://doi.org/10.1038/nclimate3286

Chern, J.-S., Ling, J., Weng, S.-L., 2008. Taiwan's second remote sensing satellite. Acta Astronaut. 63, 1305–1311. https://doi.org/10.1016/j.actaastro.2008.05.022

Choudhury, B.J., 2000. A sensitivity analysis of the radiation use efficiency for gross photosynthesis and net carbon accumulation by wheat. Agric. For. Meteorol. 101, 217–234. https://doi.org/10.1016/S0168-1923(99)00156-2

Ciais, P., Wattenbach, M., Vuichard, N., Smith, P., Piao, S.L., Don, A., Luyssaert, S., Janssens, I.A., Bondeau, A., Dechow, R., Leip, A., Smith, Pc., Beer, C., Van Der Werf, G.R., Gervois, S., Van Oost, K., Tomelleri, E., Freibauer, A., Schulze, E.D., CARBOEUROPE SYNTHESIS TEAM, 2010. The European carbon balance. Part 2: croplands. Glob. Change Biol. 16, 1409–1428. https://doi.org/10.1111/j.1365-2486.2009.02055.x

Claverie, M., Demarez, V., Duchemin, B., Hagolle, O., Ducrot, D., Marais-Sicre, C., Dejoux, J.-F., Huc, M., Keravec, P., Béziat, P., Fieuzal, R., Ceschia, E., Dedieu, G., 2012. Maize and sunflower biomass estimation in southwest France using high spatial and temporal resolution remote sensing data. Remote Sens. Environ. 124, 844–857. https://doi.org/10.1016/j.rse.2012.04.005

Coleman, K., Jenkinson, D.S., 1996. RothC-26.3 - A Model for the turnover of carbon in soil, in: Powlson, D.S., Smith, P., Smith, J.U. (Eds.), Evaluation of Soil Organic Matter Models. Springer Berlin Heidelberg, Berlin, Heidelberg, pp. 237–246. https://doi.org/10.1007/978-3-642-61094-3_17

Cong, R., Wang, X., Xu, M., Ogle, S.M., Parton, W.J., 2014. Evaluation of the CENTURY Model Using Long-Term Fertilization Trials under Corn-Wheat Cropping Systems in the Typical Croplands of China. PLoS ONE 9, e95142. https://doi.org/10.1371/journal.pone.0095142

Dai, J., Bean, B., Brown, B., Bruening, W., Edwards, J., Flowers, M., Karow, R., Lee, C., Morgan, G., Ottman, M., Ransom, J., Wiersma, J., 2016. Harvest index and straw yield of five classes of wheat. Biomass Bioenergy 85, 223–227. https://doi.org/10.1016/j.biombioe.2015.12.023

Delogu, E., 2013. Modélisation de la respiration du sol dans les agrosystèmes, Université Paul Sabatier, Toulouse III.

De Jong, J. B. R. M. (1980). Een karakterisering van de zonnestraling in Nederland.

de Noblet-Ducoudré, N., Gervois, S., Ciais, P., Viovy, N., Brisson, N., Seguin, B., Perrier, A., 2004. Coupling the Soil-Vegetation-Atmosphere-Transfer Scheme ORCHIDEE to the agronomy model STICS to study the influence of croplands on the European carbon and water budgets. Agronomie 24, 397–407. https://doi.org/10.1051/agro:2004038

Delogu, E., Le Dantec, V., Mordelet, P., Ceschia, E., Aubinet, M., Buysse, P., Pattey, E., 2017. Improved methodology to quantify the temperature sensitivity of the soil heterotrophic respiration in croplands. Geoderma 296, 18–29. https://doi.org/10.1016/j.geoderma.2017.02.017

Demarez, V., Duthoit, S., Baret, F., Weiss, M., Dedieu, G., 2008. Estimation of leaf area and clumping indexes of crops with hemispherical photographs. Agric. For. Meteorol. 148, 644–655. https://doi.org/10.1016/j.agrformet.2007.11.015

Dimassi, B., Mary, B., Fontaine, S., Perveen, N., Revaillot, S., Cohan, J.-P., 2014. Effect of nutrients availability and long-term tillage on priming effect and soil C mineralization. Soil Biol. Biochem. 78, 332–339. https://doi.org/10.1016/j.soilbio.2014.07.016

Duan, S.-B., Li, Z.-L., Wu, H., Tang, B.-H., Ma, L., Zhao, E., Li, C., 2014. Inversion of the PROSAIL model to estimate leaf area index of maize, potato, and sunflower fields from unmanned aerial vehicle hyperspectral data. Int. J. Appl. Earth Obs. Geoinformation 26, 12–20. https://doi.org/10.1016/j.jag.2013.05.007

Duchemin, B., Fieuzal, R., Rivera, M., Ezzahar, J., Jarlan, L., Rodriguez, J., Hagolle, O., Watts, C., 2015. Impact of Sowing Date on Yield and Water Use Efficiency of Wheat Analyzed through Spatial Modeling and FORMOSAT-2 Images. Remote Sens. 7, 5951–5979. https://doi.org/10.3390/rs70505951

Duchemin, B., Maisongrande, P., Boulet, G., Benhadj, I., 2008. A simple algorithm for yield estimates: Evaluation for semi-arid irrigated winter wheat monitored with green leaf area index. Environ. Model. Softw. 23, 876–892. https://doi.org/10.1016/j.envsoft.2007.10.003

Durand, Y., Brun, E., Merindol, L., Guyomarc'h, G., Lesaffre, B., Martin, E., 1993. A meteorological estimation of relevant parameters for snow models. Ann. Glaciol. 18, 65–71. https://doi.org/10.1017/S0260305500011277

Eugster, W., Moffat, A.M., Ceschia, E., Aubinet, M., Ammann, C., Osborne, B., Davis, P.A., Smith, P., Jacobs, C., Moors, E., Le Dantec, V., Béziat, P., Saunders, M., Jans, W., Grünwald, T., Rebmann, C., Kutsch, W.L., Czerný, R., Janouš, D., Moureaux, C., Dufranne, D., Carrara, A., Magliulo, V., Di Tommasi, P., Olesen, J.E., Schelde, K., Olioso, A., Bernhofer, C., Cellier, P., Larmanou, E., Loubet, B., Wattenbach, M., Marloie, O., Sanz, M.-J., Søgaard, H., Buchmann, N., 2010. Management effects on European cropland respiration. Agric. Ecosyst. Environ. 139, 346–362. https://doi.org/10.1016/j.agee.2010.09.001

Falloon, P., Smith, P., 2006. Simulating SOC changes in long-term experiments with RothC and CENTURY: model evaluation for a regional scale application. Soil Use Manag. 18, 101–111. https://doi.org/10.1111/j.1475-2743.2002.tb00227.x

Falloon, P., Smith, P., 2003. Accounting for changes in soil carbon under the Kyoto Protocol: need for improved long-term data sets to reduce uncertainty in model projections. Soil Use Manag. 19, 265–269. https://doi.org/10.1111/j.1475-2743.2003.tb00313.x

Fieuzal, R., Duchemin, B., Jarlan, L., Zribi, M., Baup, F., Merlin, O., Hagolle, O., Garatuza-Payan, J., 2011. Combined use of optical and radar satellite data for the monitoring of irrigation and soil moisture of wheat crops. Hydrol. Earth Syst. Sci. 15, 1117–1129. https://doi.org/10.5194/hess-15-1117-2011

Fieuzal, R., Marais Sicre, C., Baup, F., 2017. Estimation of corn yield using multi-temporal optical and radar satellite data and artificial neural networks. Int. J. Appl. Earth Obs. Geoinformation 57, 14–23. https://doi.org/10.1016/j.jag.2016.12.011

Fieuzal, Remy, Marais Sicre, C., Baup, F., 2017. Estimation of Sunflower Yield Using a Simplified Agrometeorological Model Controlled by Optical and SAR Satellite Data. IEEE J. Sel. Top. Appl. Earth Obs. Remote Sens. 10, 5412–5422. https://doi.org/10.1109/JSTARS.2017.2737656

Gabrielle, B., Denoroy, P., Gosse, G., Justes, E., Andersen, M.N., 1998. A model of leaf area development and senescence for winter oilseed rape. Field Crops Res. 57, 209–222. https://doi.org/10.1016/S0378-4290(97)00147-0

Gabrielle, B., Laville, P., Duval, O., Nicoullaud, B., Germon, J.C., Hénault, C., 2006. Process-based modeling of nitrous oxide emissions from wheat-cropped soils at the subregional scale: REGIONAL N_2O EMISSIONS FROM ARABLE SOILS. Glob. Biogeochem. Cycles 20, n/a-n/a. https://doi.org/10.1029/2006GB002686

Gervois, S., Ciais, P., de Noblet-Ducoudré, N., Brisson, N., Vuichard, N., Viovy, N., 2008. Carbon and water balance of European croplands throughout the 20th century: CARBON BALANCE OF EUROPEAN CROPLANDS. Glob. Biogeochem. Cycles 22, n/a-n/a. https://doi.org/10.1029/2007GB003018

Grant, R.F., Arkebauer, T.J., Dobermann, A., Hubbard, K.G., Schimelfenig, T.T., Suyker, A.E., Verma, S.B., Walters, D.T., 2007. Net Biome Productivity of Irrigated and Rainfed Maize–Soybean Rotations: Modeling vs. Measurements. Agron. J. 99, 1404. https://doi.org/10.2134/agronj2006.0308

Guo, L., Falloon, P., Coleman, K., Zhou, B., Li, Y., Lin, E., Zhang, F., 2007. Application of the RothC model to the results of long-term experiments on typical upland soils in northern China. Soil Use Manag. 23, 63–70. https://doi.org/10.1111/j.1475-2743.2006.00056.x

Hadria, R., Duchemin, B., Jarlan, L., Dedieu, G., Baup, F., Khabba, S., Olioso, A., Le Toan, T., 2010. Potentiality of optical and radar satellite data at high spatio-temporal resolutions for the monitoring of irrigated wheat crops in Morocco. Int. J. Appl. Earth Obs. Geoinformation 12, S32–S37. https://doi.org/10.1016/j.jag.2009.09.003

Hollinger, D.Y., Kelliher, F.M., Schulze, E.-D., Bauer, G., Arneth, A., Byers, J.N., Hunt, J.E., McSeveny, T.M., Kobak, K.I., Milukova, I., Sogatchev, A., Tatarinov, F., Varlargin, A., Ziegler, W., Vygodskaya, N.N., 1998. Forest–atmosphere carbon dioxide exchange in eastern Siberia. Agric. For. Meteorol. 90, 291–306. https://doi.org/10.1016/S0168-1923(98)00057-4

Huang, Y., Yu, Y., Zhang, W., Sun, W., Liu, S., Jiang, J., Wu, J., Yu, W., Wang, Y., Yang, Z., 2009. Agro-C: A biogeophysical model for simulating the carbon budget of agroecosystems. Agric. For. Meteorol. 149, 106–129. https://doi.org/10.1016/j.agrformet.2008.07.013

Jacquemoud, S., Verhoef, W., Baret, F., Bacour, C., Zarco-Tejada, P.J., Asner, G.P., François, C., Ustin, S.L., 2009. PROSPECT+SAIL models: A review of use for vegetation characterization. Remote Sens. Environ. 113, S56–S66. https://doi.org/10.1016/j.rse.2008.01.026

Kaye, J.P., Quemada, M., 2017. Using cover crops to mitigate and adapt to climate change. A review. Agron. Sustain. Dev. 37. https://doi.org/10.1007/s13593-016-0410-x

Krinner, G., Viovy, N., Noblet-Ducoudré, N. de, Ogée, J., Polcher, J., Friedlingstein, P., Ciais, P., Sitch, S., Prentice, I.C., 2005. A dynamic global vegetation model for studies of the coupled atmosphere-biosphere system. Glob. Biogeochem. Cycles 19. https://doi.org/10.1029/2003GB002199

Kuzyakov, Y., Friedel, J.K., Stahr, K., 2000. Review of mechanisms and quanti®cation of priming e ects. Soil Biol. 14.

Lagarias, J.C., Reeds, J.A., Wright, M.H., Wright, P.E., 1998. Convergence Properties of the Nelder--Mead Simplex Method in Low Dimensions. SIAM J. Optim. 9, 112–147. https://doi.org/10.1137/S1052623496303470

Lal, R., 2016. Beyond COP 21: Potential and challenges of the "4 per Thousand" initiative. J. Soil Water Conserv. 71, 20A-25A. https://doi.org/10.2489/jswc.71.1.20A

Lehuger, S., Gabrielle, B., Oijen, M. van, Makowski, D., Germon, J.-C., Morvan, T., Hénault, C., 2009. Bayesian calibration of the nitrous oxide emission module of an agro-ecosystem model. Agric. Ecosyst. Environ. 133, 208–222. https://doi.org/10.1016/j.agee.2009.04.022

Li, C., Frolking, S., Frolking, T.A., 1992. A model of nitrous oxide evolution from soil driven by rainfall events: 1. Model structure and sensitivity. J. Geophys. Res. Atmospheres 97, 9759–9776. https://doi.org/10.1029/92JD00509

Li, C., Frolking, S., Harriss, R., 1994. Modeling carbon biogeochemistry in agricultural soils. Glob. Biogeochem. Cycles 8, 237–254. https://doi.org/10.1029/94GB00767

Li, C., Frolking, S., Xiao, X., Moore, B., Boles, S., Qiu, J., Huang, Y., Salas, W., Sass, R., 2005. Modeling impacts of farming management alternatives on CO_2, CH_4, and N_2O emissions: A case study for water management of rice agriculture of China: WATER MANAGEMENT AND CHINA PADDY GREENHOUSE GAS FLUXES. Glob. Biogeochem. Cycles 19. https://doi.org/10.1029/2004GB002341

Lohila, A., Aurela, M., Regina, K., Laurila, T., 2013. Soil and total ecosystem respiration in agricultural fields: effect of soil and crop type. Plant and Soil, 251(2), 303-317.

McCree, K.J., 1974. Equations for the Rate of Dark Respiration of White Clover and Grain Sorghum, as Functions of Dry Weight, Photosynthetic Rate, and Temperature1. Crop Sci. 14, 509. https://doi.org/10.2135/cropsci1974.0011183X001400040005x

Minasny, B., Malone, B.P., McBratney, A.B., Angers, D.A., Arrouays, D., Chambers, A., Chaplot, V., Chen, Z.-S., Cheng, K., Das, B.S., Field, D.J., Gimona, A., Hedley, C.B., Hong, S.Y., Mandal, B., Marchant, B.P., Martin, M., McConkey, B.G., Mulder, V.L., O'Rourke, S., Richer-de-Forges, A.C., Odeh, I., Padarian, J., Paustian, K., Pan, G., Poggio, L., Savin, I., Stolbovoy, V., Stockmann, U., Sulaeman, Y., Tsui, C.-C., Vågen, T.-G., van Wesemael, B., Winowiecki, L., 2017. Soil carbon 4 per mille. Geoderma 292, 59–86. https://doi.org/10.1016/j.geoderma.2017.01.002

Moncrieff, J.B., Massheder, J.M., de Bruin, H., Elbers, J., Friborg, T., Heusinkveld, B., Kabat, P., Scott, S., Soegaard, H., Verhoef, A., 1997. A system to measure surface fluxes of momentum, sensible heat, water vapour and carbon dioxide. J. Hydrol. 188–189, 589–611. https://doi.org/10.1016/S0022-1694(96)03194-0

Monteith, J.L., Moss, C.J., 1977. Climate and the Efficiency of Crop Production in Britain [and Discussion]. Philos. Trans. R. Soc. B Biol. Sci. 281, 277–294. https://doi.org/10.1098/rstb.1977.0140

Osborne, B., Saunders, M., Walmsley, D., Jones, M., Smith, P., 2010. Key questions and uncertainties associated with the assessment of the cropland greenhouse gas balance. Agric. Ecosyst. Environ. 139, 293–301. https://doi.org/10.1016/j.agee.2010.05.009

Parton, W.J., Schimel, D.S., Cole, C.V., Ojima, D.S., 1987. Analysis of Factors Controlling Soil Organic Matter Levels in Great Plains Grasslands. Soil Sci. Soc. Am. J. 51, 1173–1179. https://doi.org/10.2136/sssaj1987.03615995005100050015x

Pellerin, S., Bamière, L., Launay, C., Martin, R., Schiavo, M., Angers, D., Augusto, L., Balesdent, J., Doelsch, I.B., Bellassen, V., Cardinael, R., Cécillon, L., Ceschia, E., Chenu, C., Constantin, J., Darroussin, J., Delacote, P., Delame, N., Gastal, F., Gilbert, D., Graux, A.-I., Guenet, B., Houot, S., Klumpp, K., Letort, E., Litrico, I., Martin, M., Menasseri-Aubry, S., Meziere, D., Morvan, T., Mosnier, C., Roger-Estrade, J., Saint-André, L., Sierra, J., Therond, O., Viaud, V., Grateau, R., Perchec, S.L., Savini, I., Rechauchère, O., 2019. Stocker du carbone dans les sols français, quel potentiel au regard de l'objectif 4 pour 1000 et à quel coût? 118.

Poeplau, C., Don, A., 2015. Carbon sequestration in agricultural soils via cultivation of cover crops – A meta-analysis. Agric. Ecosyst. Environ. 200, 33–41. https://doi.org/10.1016/j.agee.2014.10.024

Porter, J.R., Gawith, M., 1999. Temperatures and the growth and development of wheat: a review. Eur. J. Agron. 10, 23–36. https://doi.org/10.1016/S1161-0301(98)00047-1

Poulton, P., Johnston, J., Macdonald, A., White, R., Powlson, D., 2018. Major limitations to achieving "4 per 1000" increases in soil organic carbon stock in temperate regions: Evidence from long-term experiments at Rothamsted Research, United Kingdom. Glob. Change Biol. 24, 2563–2584. https://doi.org/10.1111/gcb.14066

Powlson, D.S., Stirling, C.M., Thierfelder, C., White, R.P., Jat, M.L., 2016. Does conservation agriculture deliver climate change mitigation through soil carbon sequestration in tropical agro-ecosystems? Agric. Ecosyst. Environ. 220, 164–174. https://doi.org/10.1016/j.agee.2016.01.005

Reichstein, M., Falge, E., Baldocchi, D., Papale, D., Aubinet, M., Berbigier, P., Bernhofer, C., Buchmann, N., Gilmanov, T., Granier, A., Grunwald, T., Havrankova, K., Ilvesniemi, H., Janous, D., Knohl, A., Laurila, T., Lohila, A., Loustau, D., Matteucci, G., Meyers, T., Miglietta, F., Ourcival, J.-M., Pumpanen, J., Rambal, S., Rotenberg, E., Sanz, M., Tenhunen, J., Seufert, G., Vaccari, F., Vesala, T., Yakir, D., Valentini, R., 2005. On the separation of net ecosystem exchange into assimilation and ecosystem respiration: review and improved algorithm. Glob. Change Biol. 11, 1424–1439. https://doi.org/10.1111/j.1365-2486.2005.001002.x

Revill, A., Sus, O., Barrett, B., Williams, M., 2013. Carbon cycling of European croplands: A framework for the assimilation of optical and microwave Earth observation data. Remote Sens. Environ. 137, 84–93. https://doi.org/10.1016/j.rse.2013.06.002

Roderick, M.L., Farquhar, G.D., Berry, S.L., Noble, I.R., 2001. On the direct effect of clouds and atmospheric particles on the productivity and structure of vegetation. Oecologia 129, 21–30. https://doi.org/10.1007/s004420100760

Saffih-Hdadi, K., Mary, B., 2008. Modeling consequences of straw residues export on soil organic carbon. Soil Biol. Biochem. 40, 594–607. https://doi.org/10.1016/j.soilbio.2007.08.022

Schmidt, M., Reichenau, T.G., Fiener, P., Schneider, K., 2012. The carbon budget of a winter wheat field: An eddy covariance analysis of seasonal and inter-annual variability. Agric. For. Meteorol. 165, 114–126. https://doi.org/10.1016/j.agrformet.2012.05.012

Smith, P., Andren, O., Karlsson, T., Perala, P., Regina, K., Rounsevell, M., Wesemael, B., 2005. Carbon sequestration potential in European croplands has been overestimated. Glob. Change Biol. 11, 2153–2163. https://doi.org/10.1111/j.1365-2486.2005.01052.x

Smith, P., Smith, J.U., Powlson, D.S., McGill, W.B., Arah, J.R.M., Chertov, O.G., Coleman, K., Franko, U., Frolking, S., Jenkinson, D.S., Jensen, L.S., Kelly, R.H., Klein-Gunnewiek, H., Komarov, A.S., Li, C., Molina, J.A.E., Mueller, T., Parton, W.J., Thornley, J.H.M., Whitmore, A.P., 1997. A comparison of the performance of nine soil organic matter models using datasets from seven long-term experiments. Geoderma 81, 153–225. https://doi.org/10.1016/S0016-7061(97)00087-6

Suleau, M., Moureaux, C., Dufranne, D., Buysse, P., Bodson, B., Destain, J.-P., Heinesch, B., Debacq, A., Aubinet, M., 2011. Respiration of three Belgian crops: Partitioning of total ecosystem respiration in its heterotrophic, above- and below-ground autotrophic components. Agric. For. Meteorol. 151, 633–643. https://doi.org/10.1016/j.agrformet.2011.01.012

Sus, O., Heuer, M.W., Meyers, T.P., Williams, M., 2013. A data assimilation framework for constraining upscaled cropland carbon flux seasonality and biometry with MODIS. Biogeosciences 10, 2451–2466. https://doi.org/10.5194/bg-10-2451-2013

Tilman, D., Balzer, C., Hill, J., Befort, B.L., 2011. Global food demand and the sustainable intensification of agriculture. Proc. Natl. Acad. Sci. 108, 20260–20264. https://doi.org/10.1073/pnas.1116437108

Tribouillois, H., Constantin, J., Justes, E., 2018. Cover crops mitigate direct greenhouse gases balance but reduce drainage under climate change scenarios in temperate climate with dry summers. Glob. Change Biol. 24, 2513–2529. https://doi.org/10.1111/gcb.14091

Vaudour, E., Gomez, C., Fouad, Y., Lagacherie, P., 2019. Sentinel-2 image capacities to predict common topsoil properties of temperate and Mediterranean agroecosystems. Remote Sens. Environ. 223, 21–33. https://doi.org/10.1016/j.rse.2019.01.006

Veloso, A., 2014. Modélisation spatialisée de la production, des flux et des bilans de carbone et d'eau des cultures de blé à l'aide de données de télédétection : application au sud-ouest de la France, Université Paul Sabatier, Toulouse III.

Veloso, A., Mermoz, S., Bouvet, A., Le Toan, T., Planells, M., Dejoux, J.-F., Ceschia, E., 2017. Understanding the temporal behavior of crops using Sentinel-1 and Sentinel-2-like data for agricultural applications. Remote Sens. Environ. 199, 415–426. https://doi.org/10.1016/j.rse.2017.07.015

Virto, I., Barré, P., Burlot, A., Chenu, C., 2012. Carbon input differences as the main factor explaining the variability in soil organic C storage in no-tilled compared to inversion tilled agrosystems. Biogeochemistry 108, 17–26.

Wang, X., Ma, M., Huang, G., Veroustraete, F., Zhang, Z., Song, Y., Tan, J., 2012. Vegetation primary production estimation at maize and alpine meadow over the Heihe River Basin, China. Int. J. Appl. Earth Obs. Geoinformation 17, 94–101. https://doi.org/10.1016/j.jag.2011.09.009

Wattenbach, M., Sus, O., Vuichard, N., Lehuger, S., Gottschalk, P., Li, L., Leip, A., Williams, M., Tomelleri, E., Kutsch, W.L., Buchmann, N., Eugster, W., Dietiker, D., Aubinet, M., Ceschia, E., Béziat, P., Grünwald, T., Hastings, A., Osborne, B., Ciais, P., Cellier, P., Smith, P., 2010. The carbon balance of European croplands: A cross-site comparison of simulation models. Agric. Ecosyst. Environ. 139, 419–453. https://doi.org/10.1016/j.agee.2010.08.004

West, T.O., Brandt, C.C., Baskaran, L.M., Hellwinckel, C.M., Mueller, R., Bernacchi, C.J., Bandaru, V., Yang, B., Wilson, B.S., Marland, G., Nelson, R.G., Ugarte, D.G.D.L.T., Post, W.M., 2010. Cropland carbon fluxes in the United States: increasing geospatial resolution of inventory-based carbon accounting. Ecol. Appl. 20, 1074–1086. https://doi.org/10.1890/08-2352.1

Williams, M., Rastetter, E.B., Fernandes, D.N., Goulden, M.L., Wofsy, S.C., Shaver, G.R., Melillo, J.M., Munger, J.W., Fan, S.-M., Nadelhoffer, K.J., 1996. Modelling the soil-plant-atmosphere continuum in a Quercus-Acer stand at Harvard Forest: the regulation of stomatal conductance by light, nitrogen and soil/plant hydraulic properties. Plant Cell Environ. 19, 911–927. https://doi.org/10.1111/j.1365-3040.1996.tb00456.x

Wolanin, A., Camps-Valls, G., Gómez-Chova, L., Mateo-García, G., van der Tol, C., Zhang, Y., Guanter, L., 2019. Estimating crop primary productivity with Sentinel-2 and Landsat 8 using machine learning methods trained with radiative transfer simulations. Remote Sens. Environ. 225, 441–457. https://doi.org/10.1016/j.rse.2019.03.002

Wu, S., Huang, J., Liu, X., Fan, J., Ma, G., Zou, J., 2012. Assimilating MODIS-LAI into Crop Growth Model with EnKF to Predict Regional Crop Yield, in: Li, D., Chen, Y. (Eds.), Computer and Computing Technologies in Agriculture V. Springer Berlin Heidelberg, Berlin, Heidelberg, pp. 410–418. https://doi.org/10.1007/978-3-642-27275-2_46

Zhan, M., Liska, A.J., Nguy-Robertson, A.L., Suyker, A.E., Pelton, M.P., Yang, H., 2019. Modeled and Measured Ecosystem Respiration in Maize–Soybean Systems Over 10 Years. Agron. J. 111, 49. https://doi.org/10.2134/agronj2018.02.0086

Supplementary material

S.1 Effect of diffuse radiation on the ELUE

The fraction of diffuse radiation affects photosynthesis (Béziat et al., 2009) and should be accounted for when simulating GPP. Furthermore, because the photosynthetic rate of leaves is usually saturated under high incoming radiation, leaves with lower irradiance will be more efficient than those with higher irradiance, and a reduction in the volume of shade leaves within the canopy should result in an increase in the efficiency of the canopy in the presence of low and diffuse radiation (Roderick et al., 2001). Thus, the photosynthetic efficiency is expected that to increase as the diffuse solar radiation increases. To quantify this effect, we used data from 5 European flux sites, including the Lamasquère and Auradé sites. The 3 other sites were Lonzee (LON) in Belgium, Grignon (GRI, located near Paris) in France and Oensingen (OEN) in Switzerland. For all sites, the ELUE increased non-linearly with the ratio of diffuse over total global radiation. As a consequence, the relationship between the effective light-use efficiency and the ratio between diffuse and direct radiation at ground level was defined as an exponential function, with parameter "b" fixed to 1.34 and parameter "a" calibrated based on the assimilation of GAI derived from satellite observations. The relationship seemed relatively generic; the correlation coefficient of the regression was 0.63.

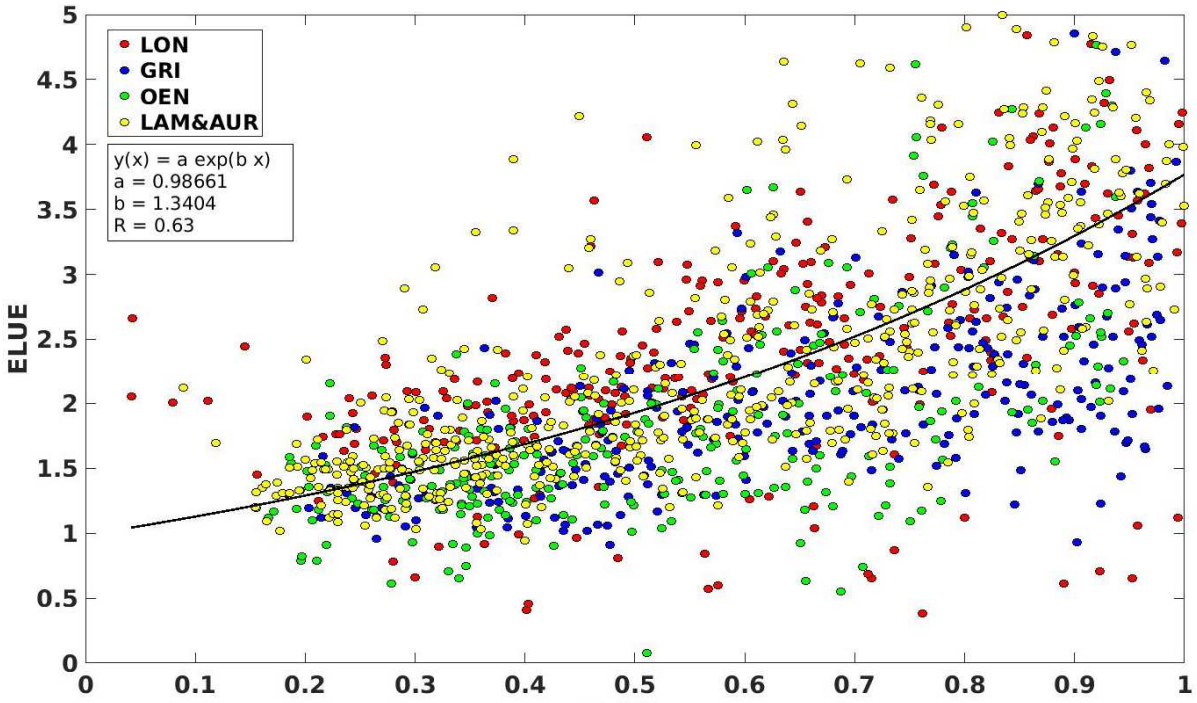

Figure S.1: Relationship between the ELUE and the ratio between diffuse (Rdf) and global (Rg) radiation measured at 5 European flux sites (Lonzée, Grignon, Oensingen, Lamasquère & Auradé)

S.2 Temporal evolutions of the in-situ and simulated net CO_2 flux components

The purpose of this section is to compare the temporal evolutions of in-situ and simulated CO_2 fluxes (GPP, R_{eco}, NEE and cumulated NEE) at FR-Lam and FR-Aur for the site years discussed in the text but not shown.

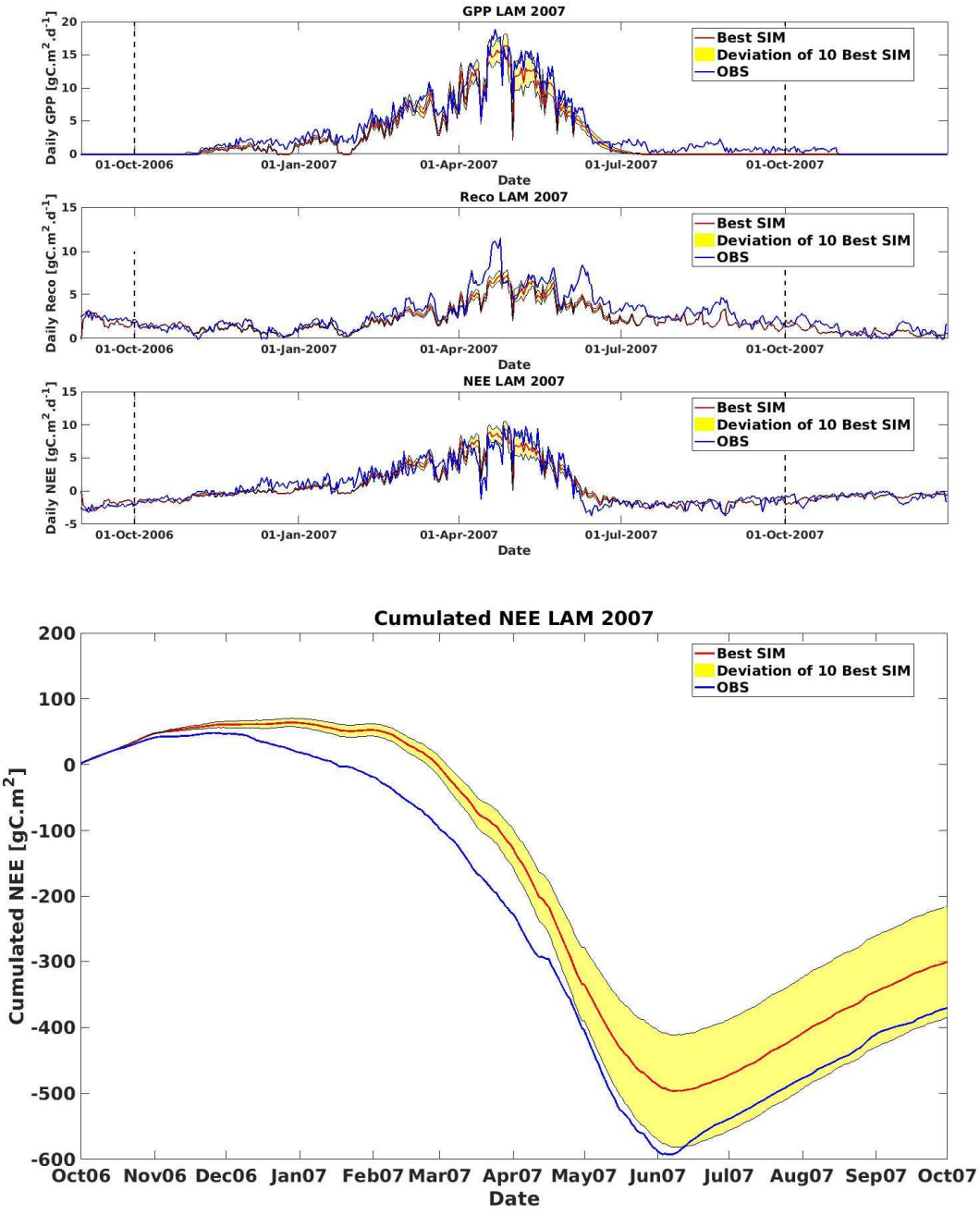

Figure S.3.1: Temporal evolution of the measured (in blue) and estimated (in red) GPP, R_{eco} and NEE, top, and cumulated NEE, bottom, for LAM2007. The yellow envelopes represent the daily standard deviation of the 10 (/30) best simulations (i.e. smaller RMSE GAI error). The vertical dashed lines define the cropping year.

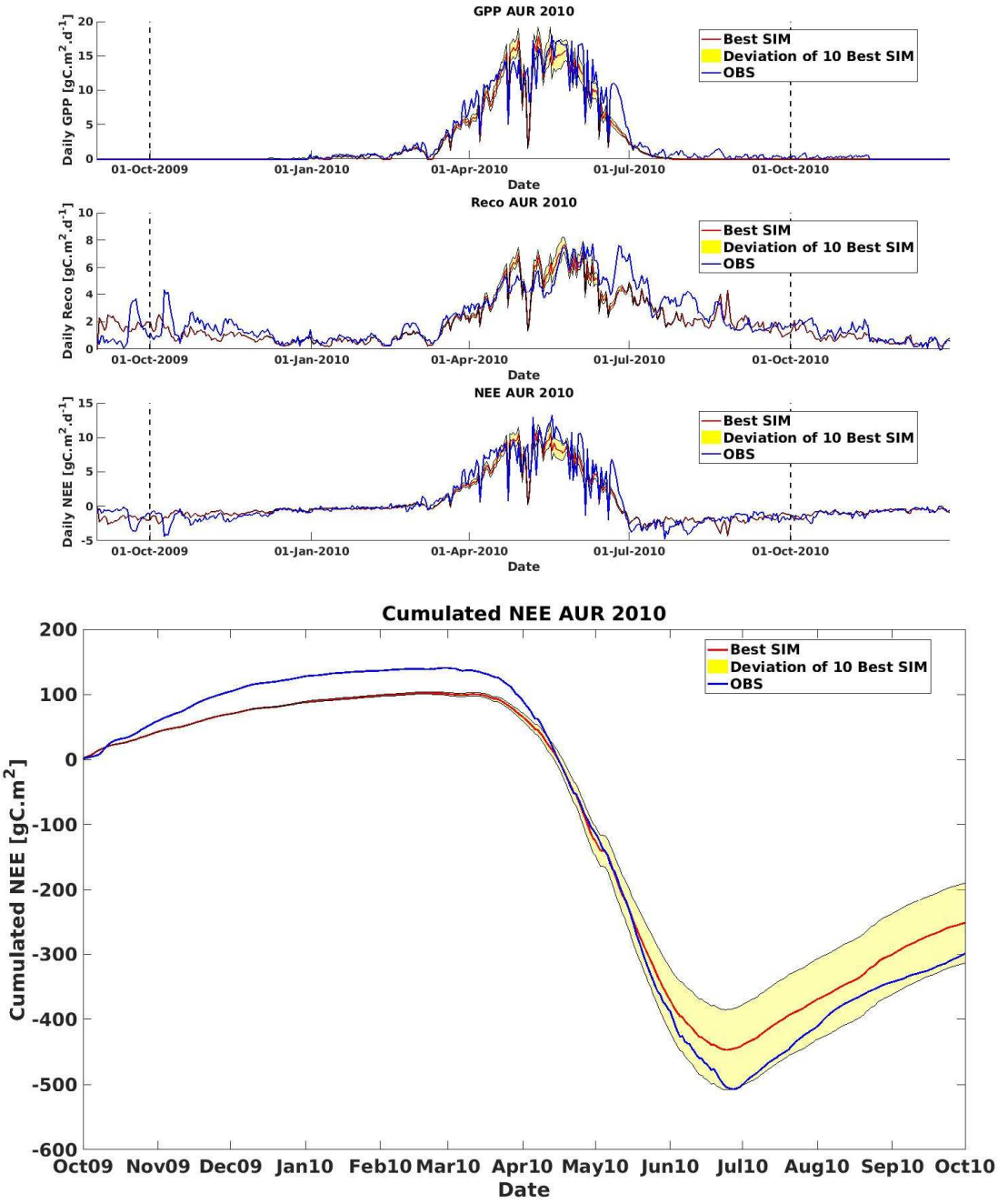

Figure S.3.2: Temporal evolution of the measured (in blue) and estimated (in red) GPP, R_{eco} and NEE, top, and cumulated NEE, bottom, for AUR2010. The yellow envelopes represent the daily standard deviation of the 10 (/30) best simulations (i.e. smaller RMSE GAI error). The vertical dashed lines define the cropping year.

1259

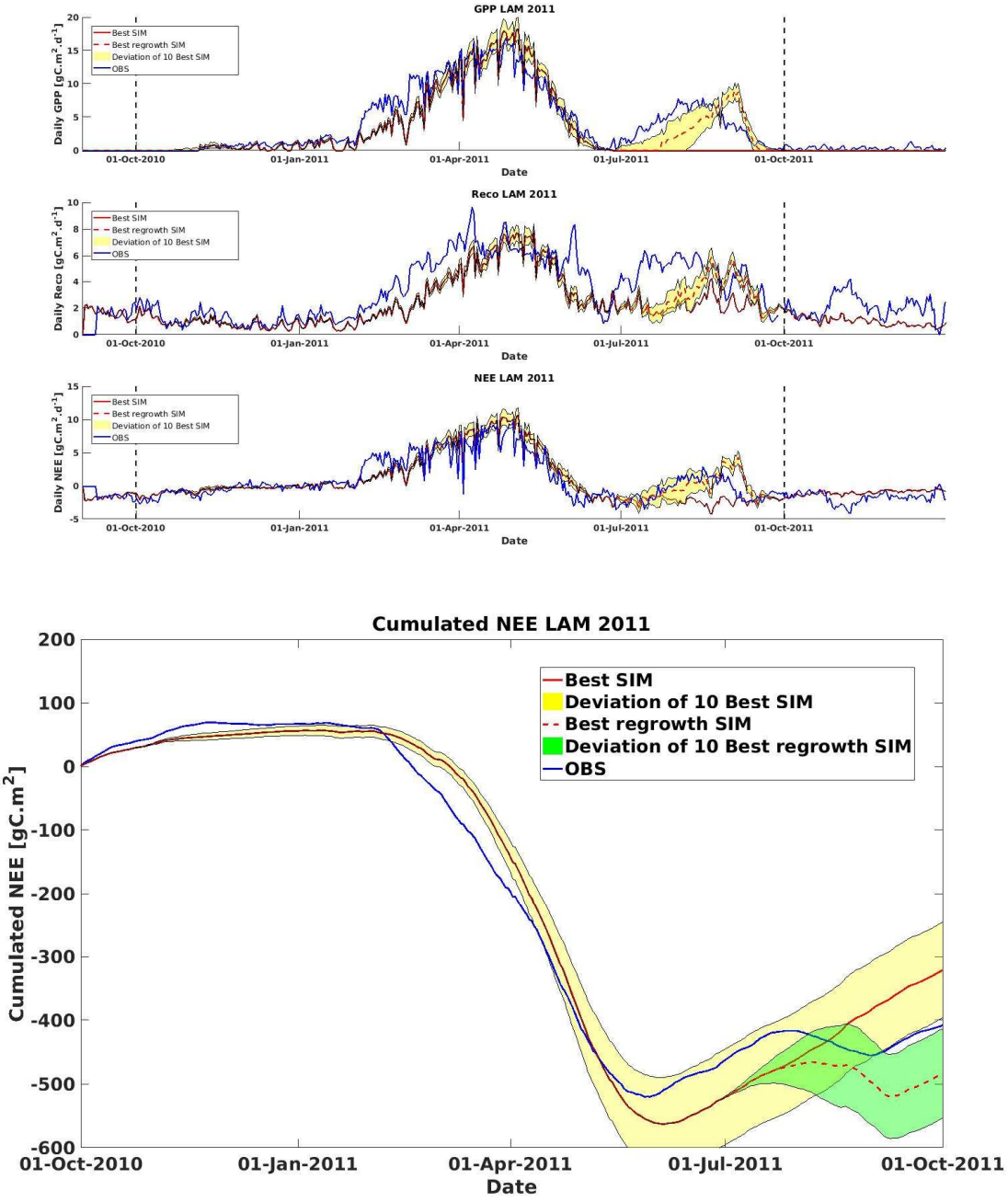

Figure S.3.3: Temporal evolution of the measured (in blue) and estimated (in red or red dashed lines) GPP, R_{eco} and NEE, top, and cumulated NEE, bottom, for LAM2011. The red/red dashed lines represent the simulations that do/do not account for re-growth and weed events. The yellow envelopes represent the daily standard deviation of the 10 (/30) best simulations (i.e. smaller RMSE GAI error).

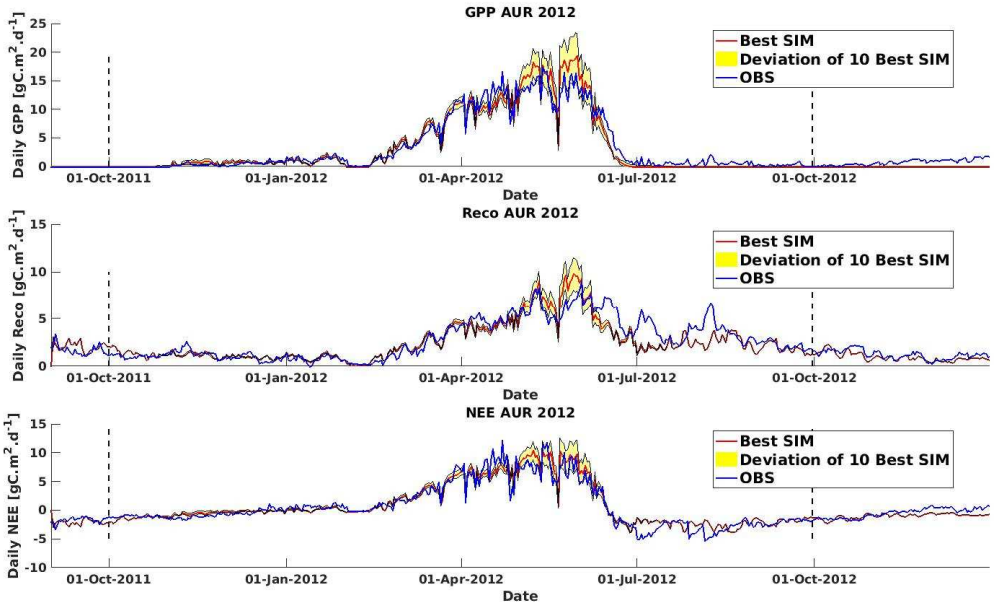

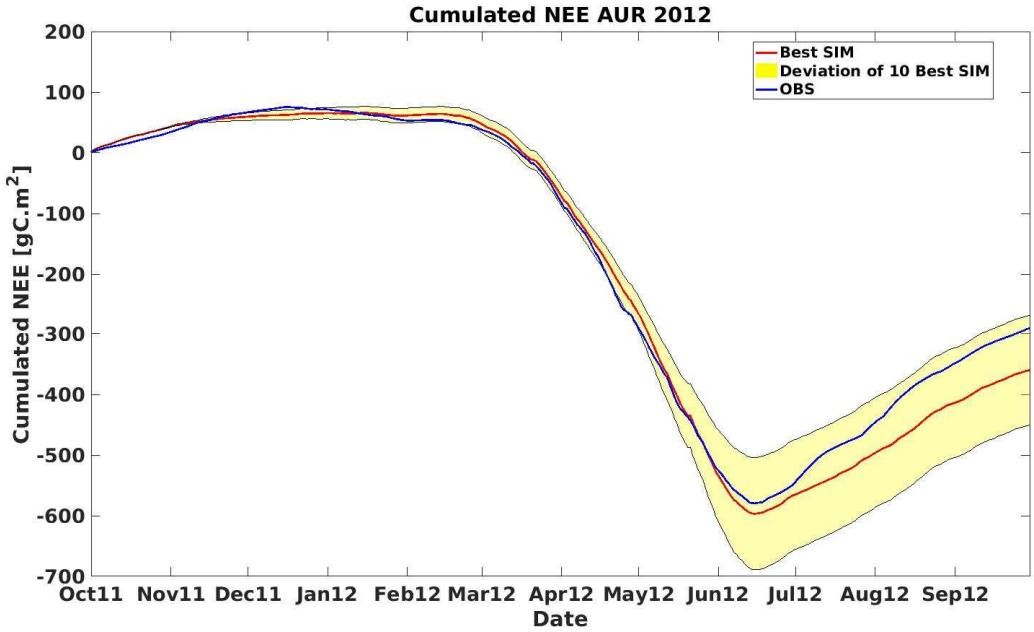

Figure S.3.4: Temporal evolution of the measured (in blue) and estimated (in red lines) GPP, R_{eco} and NEE, top, and cumulated NEE, bottom, for AUR2012. The yellow envelopes represent the daily standard deviation of the 10 (/30) best simulations (i.e. smaller RMSE GAI error). The vertical dashed lines define the cropping year.

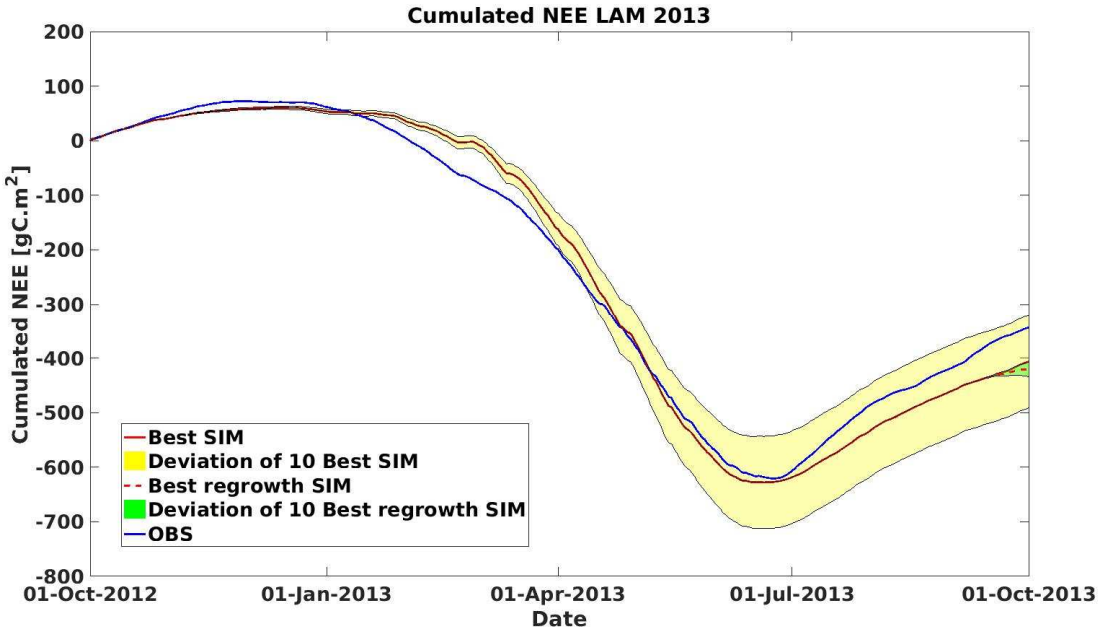

Figure S.3.5: Temporal evolution of the measured (in blue) and estimated (in red or red dashed lines) cumulated NEE for LAM2013. The red/red dashed lines represent the simulations that do/do not account for re-growth and weed events. The yellow envelopes represent the daily standard deviation of the 10 (/30) best simulations (i.e. smaller RMSE GAI error).

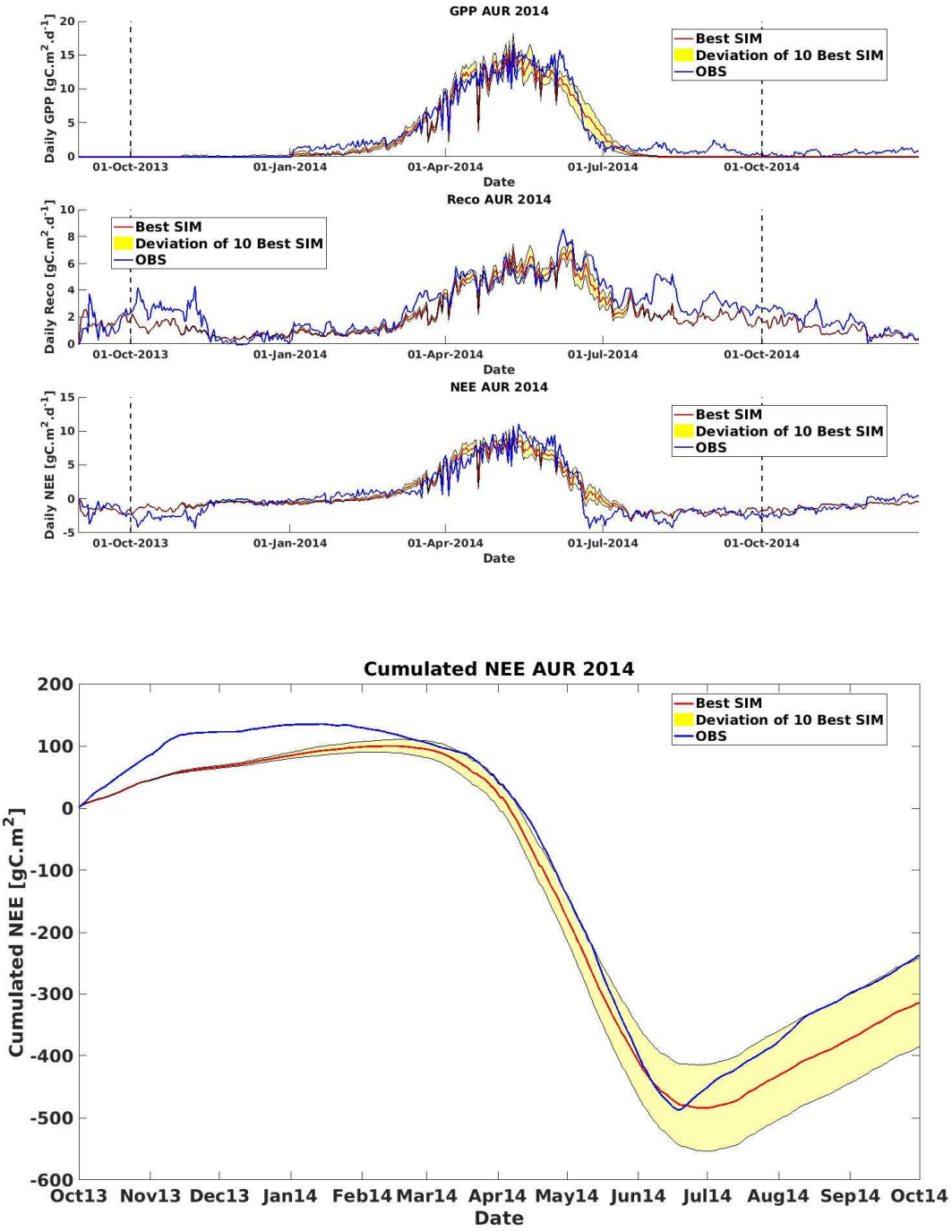

Figure S.3.6: Temporal evolution of the measured (in blue) and estimated (in red lines) GPP, R_{eco} and NEE, top, and cumulated NEE, bottom, for AUR2014. The yellow envelopes represent the daily standard deviation of the 10 (/30) best simulations (i.e. smaller RMSE GAI error). The vertical dashed lines define the cropping year.